FLEX-GEAR ELECTRICAL POWER TRANSMISSION

Final Report

(15 July 1992 through 15 September 1993)

Principal Investigator: John Vranish (Code 714)
Graduate Student: Jonathan Peritt
Advisor: Lung-Wen Tsai

NASA Grant NAG5-2004
Institute for Systems Research
University of Maryland
College Park, Maryland 20742

FLEX-GEAR ELECTRICAL POWER TRANSMISSION

Final Report

(15 July 1992 through 15 September 1993)

Principal Investigator: John Vranish (Code 714)
Graduate Student: Jonathan Peritt
Advisor: Lung-Wen Tsai

NASA Grant NAG5-2004
Institute for Systems Research
University of Maryland
College Park, Maryland 20742

Abstract

This study was conducted to develop an alternative way of transferring electricity across a continuously rotating joint, with little wear and the potential for low electrical noise. The problems with wires, slip rings, electromagnetic couplings, and recently invented roll-rings are discussed. Flex-gears, an improvement of roll-rings, are described. An entire class of flex-gear devices is developed. Finally, the preferred flex-gear device is optimized for maximum electrical contact and analyzed for average mechanical power loss and maximum stress.

For a device diameter of six inches, the preferred device is predicted to have a total electrical contact area of 0.066 square inches. In the preferred device, a small amount of internal sliding produces a 0.003 inch-pound torque that resists the motion of the device.

Acknowledgments

I extend appreciation to my advisor Lung-Wen Tsai for contributing his uncompensated time. His expertise guided me through this endeavor, especially in his innovative application of involute gear technology, which lead to the design and analysis of Pitch-Rolling-Gears.

I owe thanks to John Vranish at NASA, Goddard Space Flight Center, for his idea of flex-gears and the initiation of the grant that made this project possible. His approach as an engineer and philosophy as an inventor are inspirations to me.

Navine Bhandarkar endured countless interruptions to give me an understanding of the finite element package ABAQUS. His sincere concern for my success is gratefully acknowledged.

I owe immeasurable thanks to my parents, whose support has always been there for me. My father, who continues to be a role model in my life, offered advice for some of the project and lent his expertise in stress analysis.

I am also indebted to professors Henry Haslach, James Sirkis, Robert Sanford, and Abhijit Dasgupta for their guidance in specific aspects of the project. Thank you.

Table of Contents

List of Tables

List of Figures

Nomenclature

A_i	contact area between one planet gear and the sun gear
A_t	contact area between all planet gears and the sun gear
C	center distance between mating gears
D	width of the annulus of the sun and outer ring gears
E	modulus of elasticity (Young's Modulus)
ΔV_A	sliding velocity, relative linear velocity between the rolling contact surfaces of mating pitch-rolling-gears
F_A	gear force through pitch point P_A
F_B	gear force through pitch point P_B
N	number of teeth on each planet gear
N_A	normal force at the contact point A
N_B	normal force at the contact point B
N_i	number of teeth on gear i
R	radius of an uncompressed planet gear
R'_i	compressed contact radius of gear i
R_a	radius of the addendum circle of the planet gears
R_i	contact radius or uncompressed radius of gear i
T_{eql}	frictional torque calculated by equilibrium
T_{nrg}	frictional torque calculated by energy equivalence
V_r	relative velocity of mating gearing surfaces at their instantaneous points of contact
W	diametrical compressive force on planet gear

a	height of addendum or planet gear tooth
b	semi-width contact length
c	radial thickness of hollow planet gear
cr	contact ratio
d	axial depth of flex-gear device
f_A	friction force at the contact point A
f_A	friction force at the contact point B
n	maximum possible number of planets
p_c	contact pitch (distance between tooth centers along the contact circle) of the planet gears
p_{ci}	contact pitch (distance between tooth centers along contact circle) of gear i
p_i	pitch, distance between tooth centers along pitch circle, of gear i
q	arc of gear tooth action along the pitch circle
r'_i	compressed working pitch radius of gear i
r_i	gear pitch radius of gear i
r_{iA}	working pitch radius of gear i at the pitch point P_A
r_{iB}	working pitch radius of gear i at the pitch point P_B
t	gear tooth thickness along the pitch circle
t_a	gear tooth thickness along the addendum circle
y	length of the line of action

α	angle of gear tooth action
Δ	Hertz contact parameter

δ	total diametrical deflection of the planet gear
δ_G	global diametrical deflection of the planet gear
δ_L	local diametrical deflection of the planet gear
ϕ	pressure angle
ϕ_A	working pressure angle at the pitch point P_A
ϕ_B	working pressure angle at the pitch point P_B
ϕ_a	pressure angle at the top of the gear tooth with respect to the gear tooth
γ	angle that a planet gear consumes in the annulus
κ	curvature of the planet gear
λ	ratio of the duration of rolling surface contact of a pitch-rolling-gear to that of a ring
μ	coefficient of friction
ν	Poisson's ratio
ρ	radius of curvature of the planet gear at the contact regions
σ_i	normal stress in the i direction (i-normal stress)
τ	shear stress
υ	radial deflection of a planet gear
$\omega_{i/j}$	angular velocity of body i with respect to body j

CHAPTER 1

INTRODUCTION

The transfer of electricity across continuously rotating joints is especially important in robot joints and brush-type motors. Traditionally, wires, brushes or slip rings, and electromagnetic couplings accomplish this task. Wires commonly span robot joints, restricting their motion and adding weight. Brushes or slip rings are used in brush motors, incurring wear and causing arcing. Electromagnetic couplings are used in brushless motors, adding weight and creating significant power loss. Flex-gears are developed herein, as an alternative to these methods of transferring electricity across continuously rotating joints.

Wires, spanning robot joints, often transfer significant electrical power for lower arm motors and end effectors. The result is a heavy joint whose range of motion is limited by these

wires. Furthermore, these wires undergo fatigue that is difficult to predict, thereby putting the reliability of the robot joint into question. According to John Vranish at NASA, Goddard Space Flight Center:

> "The Flight Telerobotic Servicer (FTS) project demonstrated, in space robotics, that cables dominate wrist size, weight, and complexity; and present the risk of snagging and fatiguing while limiting motion. . . The Alpha joint on Space Station Freedom illustrates the need for cableless power transfer across a revolute joint. . . The Articulated Calibration Experiment (ACE) for Earth Observation System (EOS) demonstrated the need for cableless power and signals across slow speed translational joints."

Brushes or slip rings were used or proposed instead of wires in many of these applications.

Brushes or slip rings present a problem for electrical power transfer, particularly in space applications. Without atmosphere, especially moisture, brushes have no lubrication and wear out quickly. The particles from wear are potential contaminants to other parts of the spacecraft. These particles increase arcing which further destroys the slip ring surface [Holm, 1967]. Furthermore, arcing generates debris that can short circuit electrical components and damage sensitive optical instruments.

An electro-magnetic coupling, such as a transformer, can be used to transfer electrical power. But, a transformer has a high

weight to power ratio and incurs significant electrical loss. Electromagnetic couplings are used in brushless motors to circumvent the problems associated with brushes in brush type motors. For this reason, brushless motors are predominantly used in space applications. However, brushless motors are incapable of exerting high torque at low speeds, as brush motors can. High torque at low speed was necessary for NASA projects, such as, Solar Max, COBE, XTE, EOS, Space Station Freedom, and FTS.

1.1 Background

Severe problems, especially in space applications, are associated with the traditional methods of transferring electricity across continuously rotating joints. Better alternatives such as roll-rings and flex-gears were conceived, previous to this thesis, to survive a space vacuum environment.

1.1.1 Roll-rings

Roll-rings were developed by Sperry Corporation [1981] to conduct electrical power across a continuously rotating joint with little wear. The roll-ring device shown in Figure 1.1 employs one or more flexible hollow *planets* to conduct electricity between two concentrically rotating conductors called *sun* and *ring* [Porter, 1985]. The roll-ring device incurs much less wear than brushes and slip rings. Each planet conducts up to one Ampere of current, according to the inventor of roll-rings, Pete Jacobson.

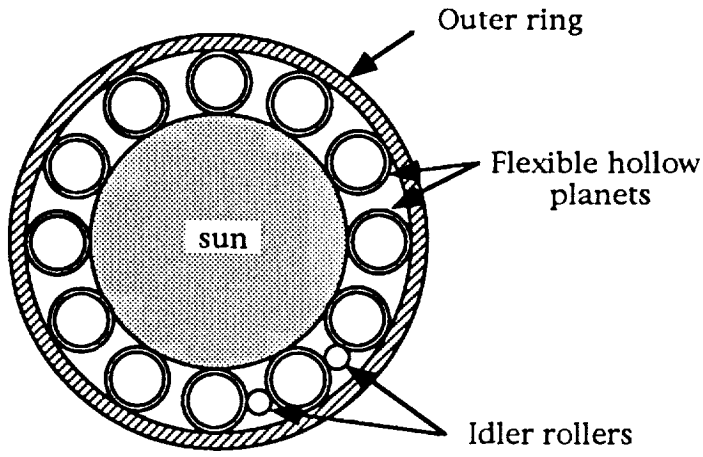

Figure 1.1: Roll-ring Device

The flexible planets of a roll-ring device eventually run into one another by *walking* (a result of micro slip) or *jerking* out of position. The result is extreme wear between the planets. One solution has been to run a single planet per roll-ring device, drastically reducing the current-carrying capability of the device. Another solution has been to separate the planets with idler rollers, as shown in Figure 1.1, or more complex caging schemes. This solution increases the complexity of the device. Furthermore, the addition of small parts prevents future reduction in the size of the device.

1.1.2 Standard Gear Flex-gears

The flex-gear device, shown in Figure 1.2, was conceived by John Vranish at NASA, Goddard Space Flight Center, as a planetary gear device whose planets maintain their own position by gear meshing. Referring to Figures 1.1 and 1.2, flex-gears differ from roll-rings only by having gear teeth. Hollowed for additional

flexibility, the planet gears are compressed in the annulus of their sun and ring gears similarly to the planets of the roll-ring device to maintain electrical contact.

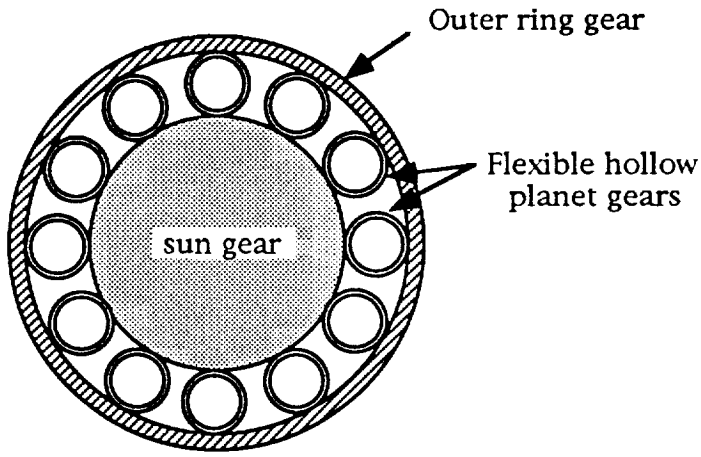

Figure 1.2: Flex-gear Device (gear teeth are not shown)

Standard gear planet gears, by having multiple tooth contact, offer more regions of contact with their sun and ring gears than the planets of a roll-ring device. This multiple tooth contact is quantified by *contact ratio*, formally defined in Chapter 2. The contact ratio is simply the average number of teeth in contact between mating gears, throughout gear meshing.

The contact ratio of a gear with a 20° pressure angle can range from 1.0 to 1.97 [Cowie, 1961]. Since a contact ratio of 1.9 means an average of 1.9 teeth in contact with the mating gear, planet gears of a flex-gear device have an average of 90% more contact regions than the planets of a roll-ring device. Thus, a flex-gear device has the potential for offering a higher current-carrying capability than the roll-ring device. However, the

number of contact regions alone does not determine current-carrying capability. More important are the contact area and pressure of those contact regions.

Increasing the electrical contact area and pressure of the planets in a flex-gear (or roll-ring) device can be accomplished by simply increasing the compression of the planet gear in the annulus of the sun and outer ring gears. If excessively compressed in the annulus, standard planet gears are subject to severe wear and mechanical power loss. Yet, if insufficiently compressed in the annulus, standard gear planet gears serve as poor electrical conductors due to low contact area and pressure. For these reasons, standard gear planet gears are judged to make relatively poor conductors in a flex-gear device. A search for other types of gears to conduct electricity in a flex-gear device is warranted.

1.2 Objectives

The objective of this research is to design a (non-standard) flex-gear device that can transfer sufficient current, while incurring little wear. It is not surprising that standard gears are not well suited for the transfer of electrical power, since they were designed to transfer mechanical power. A new class of gears is developed in this work to transfer electrical power. These gears maintain robust electrical contact, while maintaining their own position in a flex-gear device.

The objectives for the design of the optimum flex-gear device are as follows:

1. Design a flex-gear device with planets that maintain their own position in the annulus of the sun and ring gears. By maintaining their own position, no additional parts, such as caging or idler wheels, are necessary to separate the planets. Multiple planets can be used to increase the current-carrying capability of the device without the danger of planet collisions.
2. Maximize the contact area between the planet gears and their sun and ring gears to further increase the current-carrying capability of the flex-gear device.
3. Insure a contact pressure, between gears, in the order of 35,000 psi. This is the approximate contact pressure between the planets and the sun and outer ring of the roll-ring device, according to the inventor of roll-rings, Pete Jacobson.
4. Minimize wear by minimizing sliding, especially on the surfaces of electrical contact. According to Holm [1967], wear is significantly increased between sliding surfaces if electricity is flowing through the interface.

1.3 Organization of Thesis

In Chapter 2, various types of non-standard planet gears are developed for the flex-gear device, according to the objectives of Section 1.2. A promising non-standard gear, called the pitch-

rolling-gear, is recommended for further study. Pitch-rolling-gears are chosen as the preferred gears for the flex-gear device at the end of Chapter 2. In Chapters 3 through 6, flex-gear design and analysis is illustrated through a specific example of a flex-gear device. An outer ring diameter of approximately six inches is imposed on the example device, since this is a reasonable size for a robot joint. Standard casting Beryllium Copper alloy* is used for all the gears in the example device. Recommended for electrical contacts, Be-Cu alloys also have excellent spring characteristics necessary for flex-gears. Furthermore, various Be-Cu alloys posses a higher strength than some steels.

In Chapter 3, the optimal diameter of the planet gears are determined by maximizing their contact area for the flow of electricity. Two models are developed to accomplish the optimization of planet size. A closed-form model employs the Hertz contact theory to model the regions of contact and the theory of ring deflection, as presented by Timoshenko [1936] to model the deformation of each planet away from the contact region. At the end of Chapter 3, the results of a finite element model are compared to those of the closed-form model.

In Chapter 4, the tooth height (and corresponding tooth thickness) of the planet gears is determined by maximizing the duration of electrical contact of the planet gears with the sun and ring gears. The optimization of planet contact employs the

* Since Beryllium Copper alloys are toxic, OSHA has specific requirements regarding their machining and processing.

technology of standard involute gears, as presented by Kimbrell [1991]. The characteristics of pitch-rolling-gears are explained and applied to flex-gear devices. The specifications for two example devices are presented, from which a preferred device is chosen.

Chapter 5 explains the kinematic and kinetic analyses of the preferred device. From these analyses, the torque required to drive the sun gear against sliding friction is estimated, and the stresses within the gears are calculated. In Chapter 6, the major contributions of this work are summarized and future work is recommended.

CHAPTER 2

DEVELOPMENT OF CONCEPT

In section 2.1, non-standard gears are developed for the flex-gear device, in accordance with the objectives listed in Section 1.2. The application of these non-standard gears to flex-gear devices is discussed in Section 2.2. For clarity, the flexibility of the gears will be ignored in the first section of this chapter, and discussed in Section 2.2, entitled Configurations.

2.1 Gear Development

Roll-rings sustain robust electrical contact, but cannot maintain their positions in their annulus without the help of idler rollers. Standard gear flex-gears maintain their own position in their annulus, but make poor electrical contact because of the low contact pressure and excessive wear between teeth.

2.1.1 Rolling-gears

Combining the advantages of both the roll-ring and the standard gear flex-gear, the *rolling-gear* was conceived as shown in Figure 2.1. A rolling-gear is simply a roll-ring with gear teeth added to prevent uncontrolled sliding. Roll-rings and standard gear flex-gears each has only one type of contact surface. Roll-rings have surfaces for electrical contact. Standard gear flex-gears have tooth surfaces for gearing that are also employed for electrical contact. Rolling-gears, however, have two entirely different types of contact surfaces: one to transfer electricity and the other to maintain the position of the gear, as shown in Figure 2.1.

The *rolling contact surfaces* are designed to transfer electricity. At least one of the two mating rolling contact surfaces is flexible and forced against its mating surface to produce sufficient contact area and pressure for electrical flow. To minimize wear, these surfaces are designed to roll rather than slip, and are therefore called rolling contact surfaces. The second type of contact surface maintains the position of the rolling-gear in the annulus. These surfaces, called *gearing surfaces*, are allowed to slide relative to each other, similar to the gearing surfaces of standard gears. Nevertheless, these surfaces will not wear severely if the contact pressure between them is low, as expected. Most of the electricity is expected to be carried by the rolling contact surfaces, since they are designed for low electrical resistance with high contact pressure and area.

If gear teeth are added to the planets, corresponding valleys must be added to the ring and sun, and visa versa. Figure 2.1 shows a rolling-gear with arbitrarily chosen valley and gear tooth shapes. The rolling-gear can slide somewhat freely between the gear teeth. Like a roll-ring, the rolling-gear is held in position mostly by the friction between the rolling contact surfaces, rolling over the gear teeth without making contact. Should slipping occur between the rolling contact surfaces by the rolling-gear walking or jerking out of position, the gear teeth reposition the rolling-gear.

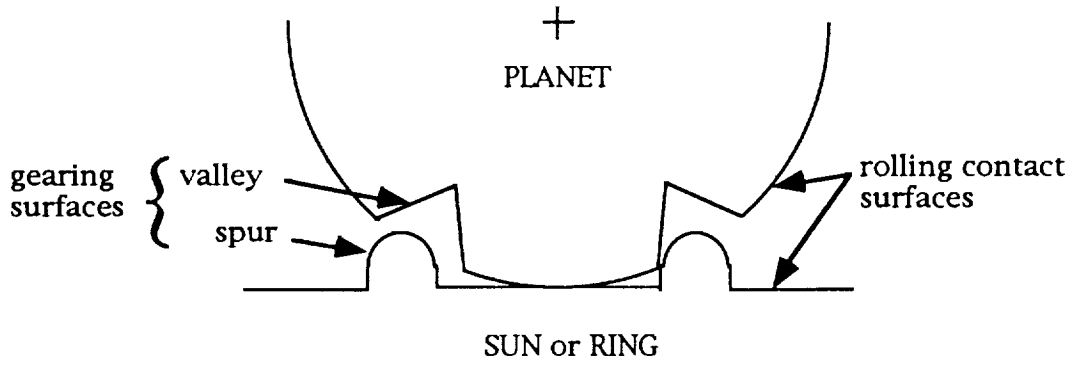

Figure 2.1: A Rolling-gear

Upon repositioning, sliding occurs between both rolling and gearing surfaces. Sliding between the rolling contact surfaces can contribute to severe wear and mechanical power loss because of high contact pressure and area. To diminish wear and mechanical power loss, a search began for gear tooth and valley shapes that would minimize sliding on the rolling contact surfaces. Candidate gear tooth curves included simple shapes like those shown in

Figure 2.1 and those common to gear technology, such as cycloids and involutes. A special application of involute curves reduces the sliding on the rolling contact surfaces to zero†. This application will be explained in the following subsection. A similar application of any conjugate gear pair reduces sliding between the rolling contact surfaces to zero. A conjugate gear pair is any pair of gear curves that exhibit conjugate action, as defined in the following subsection. Nevertheless, involute gear curves are used, henceforth, for the gearing surfaces of rolling-gears. This special configuration of rolling-gears, called *pitch-rolling-gears*, is explained in the following subsection.

2.1.2 Pitch-rolling-gears

Since the development of pitch-rolling-gears requires an understanding of involute gear technology, a brief review is presented. For a more thorough understanding of involute gear technology, the reader is referred to Shigley and Mischke [1989] or Kimbrell [1991].

Meshing between two standard involute gears is shown in Figure 2.2a. Initial gear contact is made at point A. A combination of sliding and rolling occurs between the mating teeth as the point of instantaneous contact follows the *pressure*

† Contribution of professor Lung-Wen Tsai.

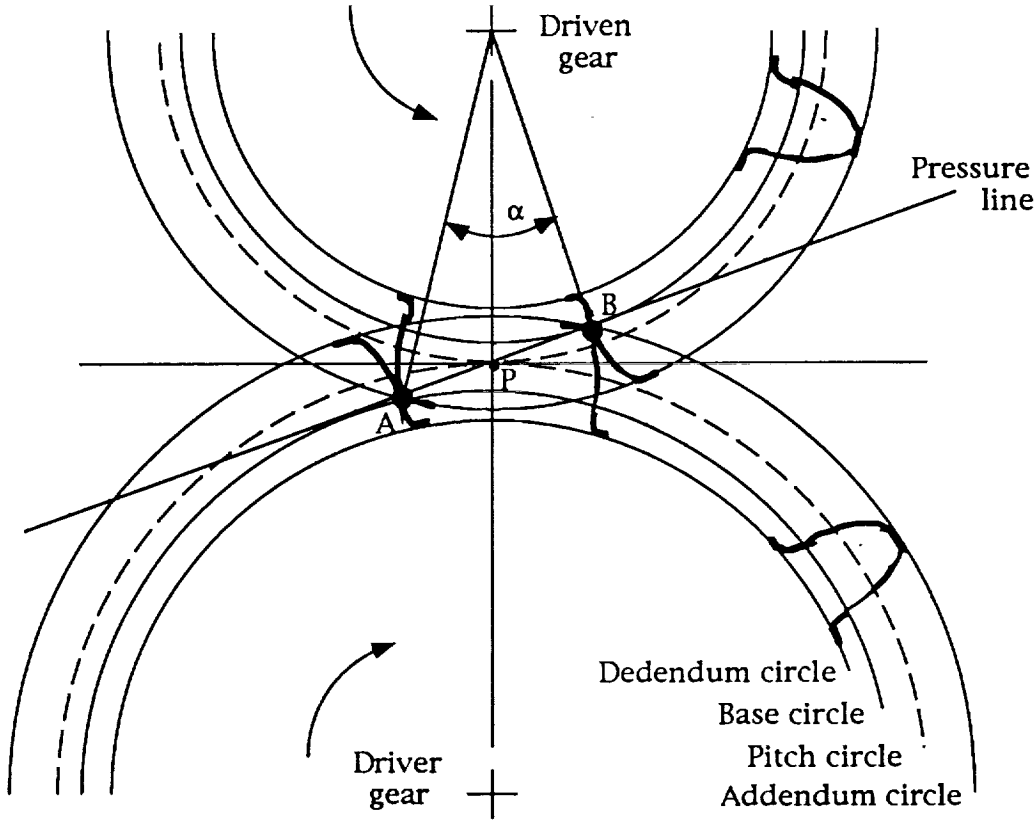

(a) Meshing

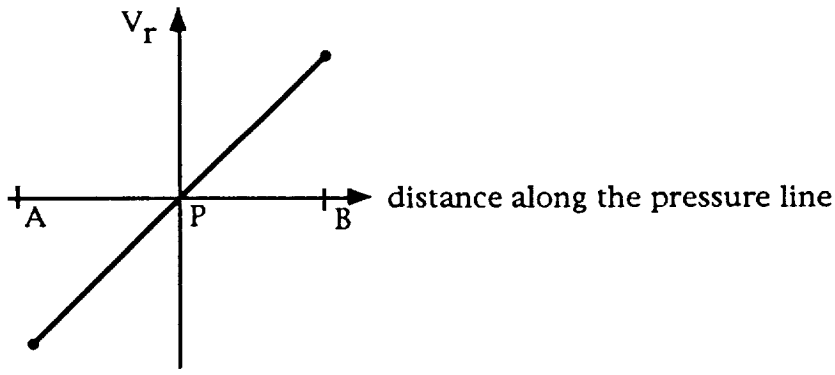

(b) Sliding between Gearing Surfaces

Figure 2.2: Standard Involute Gear Action

line until separation at point B. The section of the pressure line between points A and B is called the *line of action*, and the angle α is referred to as the *angle of action*. The *dedendum circle* marks the roots of the gear teeth, while the *addendum circle* marks their tips. The *base circle* is tangent to the pressure line and marks the diameter from which involutes are drawn to form gear teeth. The pitch circle is defined as the circle that passes through the pitch point P.

The relative velocity between mating gear teeth, at their point of instantaneous contact, is a measure of sliding. In Figure 2.2b, the relative velocity V_r is zero at the pitch point P, indicating pure rolling at that point. This means that an involute gear rotates as if it were rolling on the imaginary pitch circle of its mating gear, thereby transmitting a constant angular velocity. The transmission of constant angular velocity is characteristic of involute gears and is referred to as *conjugate action*. By exploiting conjugate action, sliding can be eliminated on the rolling contact surfaces of pitch-rolling-gears.

The exploitation of conjugate action is implemented by the formation of special teeth, as shown in Figure 2.3. A *dedendum gear tooth* is formed by cutting off the addendum of a standard gear tooth. An *addendum gear tooth* is formed by filling in its dedendum. Upon meshing, the cut-off portions of a *dedendum gear* roll on the filled-in portions of an *addendum gear* to produce *rolling contact*. These surfaces are called *rolling contact surfaces* like those of a rolling-gear. Since these rolling

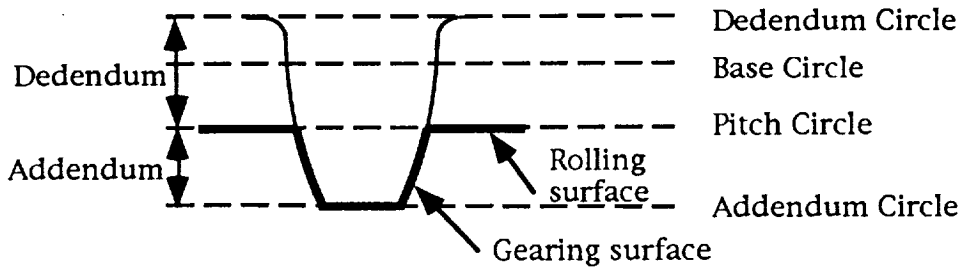

(a) A Fragment of an Addendum Gear

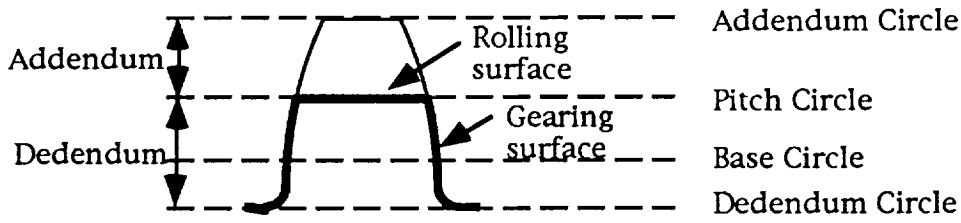

(b) A Fragment of a Dedendum Gear

Figure 2.3: Pitch-rolling-gear Teeth

contact surfaces lay on the pitch circles of gears, this type of gear is called a pitch-rolling-gear. Meanwhile, the contact between the gearing surfaces maintains conjugate action to ensure pure rolling on the rolling contact surfaces.

In Figure 2.4a, the dedendum gear teeth have been widened and the addendum gear teeth slimmed to maximize the duration of contact between the rolling contact surfaces. The leftmost addendum gear tooth makes initial contact with the dedendum gear at point A. Sliding and rolling occurs between the mating teeth along the line of action until separation at the pitch point P, similar to standard gear meshing. Figure 2.4b shows the sliding, or relative velocity V_r, between the gearing surfaces of mating pitch-rolling-gears. Notice how this compares to the sliding or relative velocity of standard gears in Figure 2.2b.

To further increase the duration of contact between the rolling contact surfaces, the pitch-rolling-gear teeth are spaced far apart. Tooth spacing is indicated by contact ratio. The *contact ratio* is defined in Subsection 1.1.2 as the average number of teeth, in contact, between mating gears. Formally, the contact ratio cr is defined as

$$cr = \frac{q}{p} \tag{2.1}$$

where p is the pitch or distance between tooth centers along the pitch circle, and q is the arc of tooth action or the arc length along the pitch circle in the angle of tooth action α. Standard

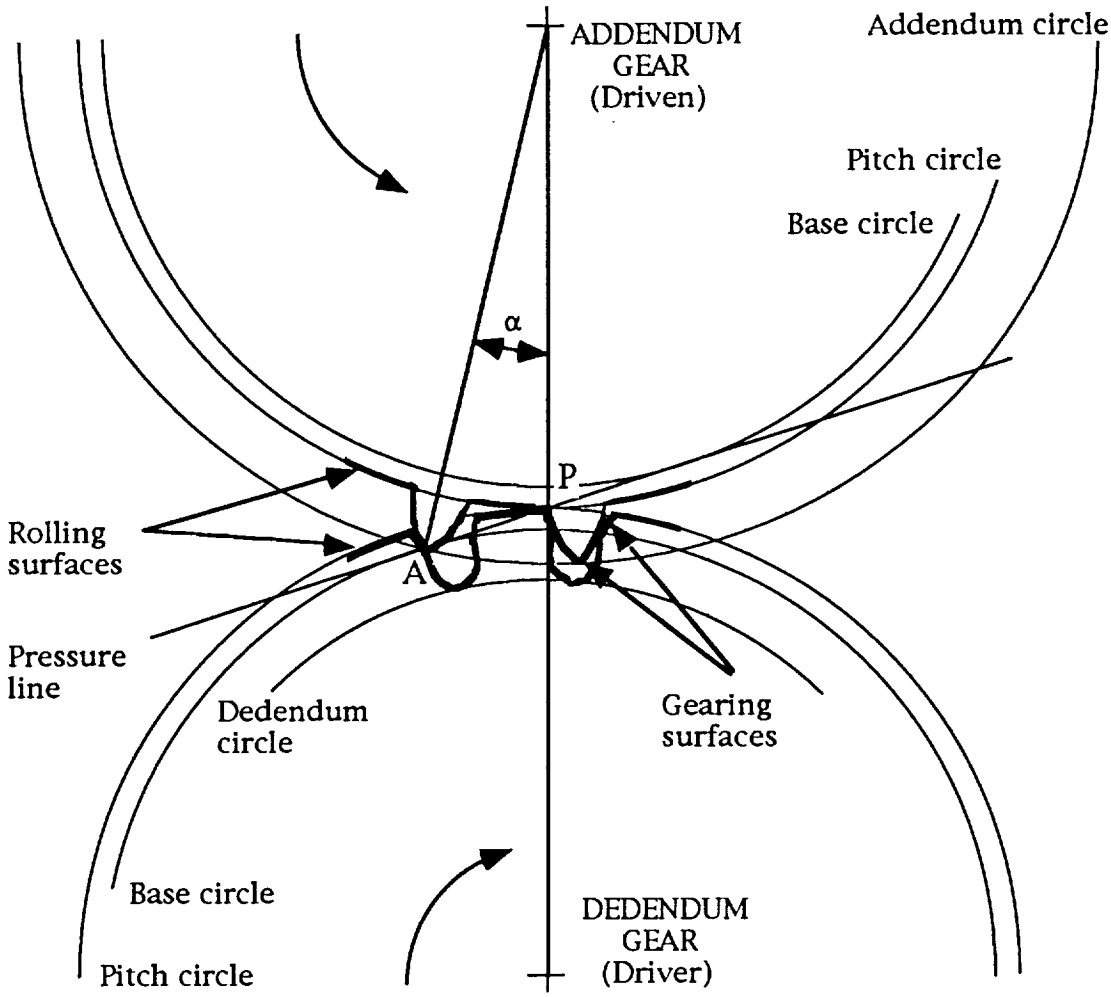

(a) Meshing

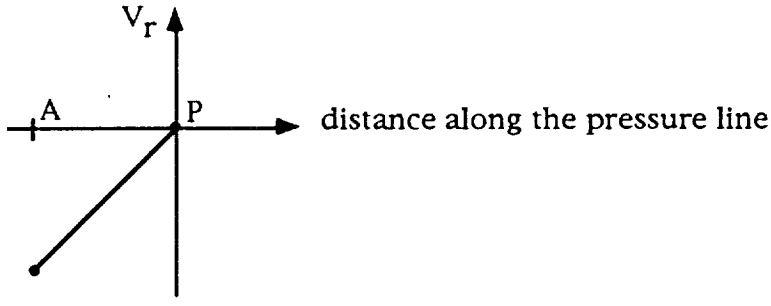

(b) Sliding between Gearing Surfaces

Figure 2.4: Pitch-rolling-gear Action

gear teeth are spaced more closely so that adjacent teeth share mechanical loads. The resulting contact ratios of standard gears are commonly between 1.2 and 1.7. Since pitch-rolling-gears are designed to carry little mechanical load, a contact ratio near 1.0 is used to maximize tooth spacing. Gear tooth size and spacing will be further studied in chapter 4 to maximize the duration of contact between the rolling contact surfaces of pitch-rolling-gears.

2.2 Configuration

To apply pitch-rolling-gears to the flex-gear device, shown in Figure 1.2, choices of flexibility (flexible or non-flexible) and gear type (addendum or dedendum) must be made for the sun, ring, and planet gears.

2.2.1 Flexibility

Until now, it has been assumed that the planet of a flex-gear device was the only flexible element, and hence, was itself called the flex-gear. But, in fact, any one or more of the gears in the planetary gear device can be flexible.

The sun and ring gears will be attached, respectively, to the inside (shaft) and outside (housing) of a revolute joint. These attachments would be significantly more complex and space consuming if the sun or ring gears were also flexible. Conversely, the planet gears are free from attachment. They are constrained in the radial direction by the sun and ring gears and in the axial

direction by electrically insulating barriers, such as ceramic plates. Furthermore, the independence of flexible planets from each other, and from other parts, improves the reliability of the device. If one flexible planet is flawed, the device may still be effective.

Finally, flexible planets have the potential for ease of manufacture. For example, tubular shapes, like hollow planets, can be made by extrusion or tube shaping. For these reasons, flexible planets with non-flexible or solid sun and outer ring gears are chosen for the preferred configuration of the flex-gear device. Accordingly, the flexible planets, themselves, are sometimes referred to as flex-gears, and the device is referred to as a flex-gear device.

Having chosen the configuration of the flex-gear device in terms of flexibility, the choice of gear type remains to be made. In the next subsection, the choice of gear type is discussed.

2.2.2 Gear Type

Planet gears, which roll in the annulus of their sun and ring gears, can be addendum or dedendum gears. Since addendum gears mesh only with dedendum gears, the choice of the planet gear type determines the mating gear type for the sun and ring gears. As shown in Figure 2.3, addendum gear teeth lie outside the pitch circle, while dedendum gear teeth lie inside. So, for equal pitch diameters, a dedendum gear is smaller than an addendum gear. This allows more dedendum gears to be packed in the same size

annulus, providing more contact area for the flow of electricity. However, for a planet diameter twenty times the tooth height, this effect is small. Tooth height is discussed in Section 4.1.

A flexible addendum gear resembles a ring with spurs, while a flexible dedendum gear resembles a corrugated ring. Because of its shape, a flexible addendum gear is thought to be easier to design, test, and prototype than a flexible dedendum gear. Both offer the same duration of electrical contact between gear teeth. Hence, flexible addendum planet gears and solid dedendum sun and ring gears constitute the preferred configuration of the flex-gear device.

The design of this configuration is centered on the design of the flexible addendum planet. The size and gear tooth specifications of the solid dedendum sun and ring gears are determined by the size, the extent of compression, and the gear tooth specifications of the planet. The size and extent of compression of the planet gear are discussed in Chapter 3. The gear teeth of the planet gear are considered in Chapter 4.

CHAPTER 3

DESIGN OF A FLEXIBLE PLANET

To maximize the current-carrying capability of the preferred configuration of a flex-gear device, the contact between the rolling contact surfaces of the gears must be optimized. A flexible addendum planet gear is simply a ring with gear teeth. To investigate its rolling surface contact with the sun and ring gears, gear teeth will be ignored, in this chapter. The resulting flexible planet will be sized, so that the flex-gear device attains maximum current-carrying capability. To model current-carrying capability of a flexible planet compressed in the annulus of its sun and ring, the physics of contact must be studied. Several types of electrical contacts are discussed in the following paragraphs.

The current-carrying capability of the contact between a brush and a metal ring may be established by its cross sectional

area and contact pressure [Still, 1916]. However, electricity only flows between the brush and the ring through contact of surface asperities. The area of asperity contact is often one thousand times less than the cross sectional area of the brush [Holm, 1967]. As a result, the average contact pressure of the asperities is one thousand times higher than the contact pressure calculated as if the entire brush were in contact. The phenomenon of asperity contact is theoretically true of any contact, and even more so for brush contact since the contact pressure is typically as low as 1 or 2 pounds per square inch of the brush cross section [Still, 1916].

Unlike that of a brush, the contact between two spheres incurs significant contact pressure. For this case, Holm [1967] takes the electrical or asperity contact area as the entire contact area, which is predicted by the Hertz contact theory.

Finally, a thin ring makes contact as shown in Figure 3.1a. A thinner ring would *globally* flatten as shown in Figure 3.1b, substantially increasing contact area while decreasing contact pressure. Because of low contact pressure, the contact of a thinner ring is not expected to have a higher current carrying capability than that of a thicker ring.

Consider the flex-gear device shown in Figure 3.2. The compression or deflection of the planet, shown in Figure 3.2a, is exaggerated. The uncompressed planet is shown in Figure 3.2b,

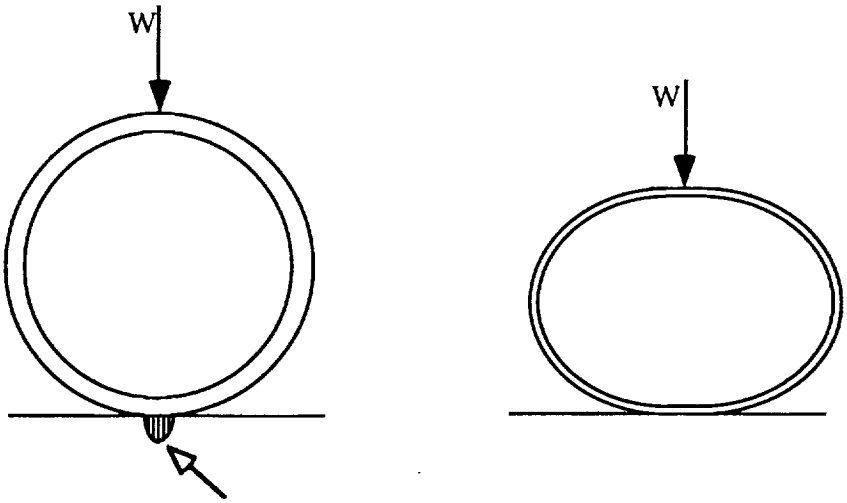

(a) Thin Ring
no global flattening

(b) Thinner Ring
globally flat

Figure 3.1: Contact Load on Rings in Diametrical Compression

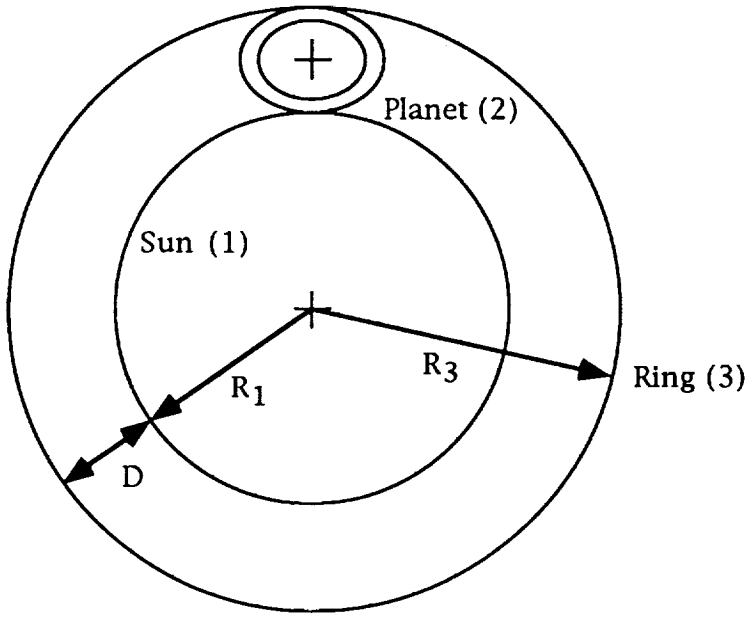

(a) Flex Gear Device without Teeth

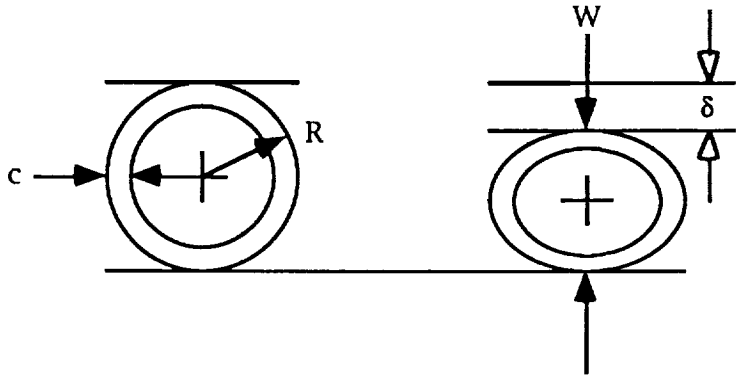

(b) Flex-gear Planet without Teeth

Figure 3.2: Flex-gear Nomenclature

where the radius R and thickness c are defined. Applying a diametrical force W in the plane of the page produces the planet deflection δ. The axial depth of the planet comes out of the page perpendicularly and is denoted by d (not shown).

From Section 1.2, the objective of the optimization of planet size is to maximize the contact area for the flow of electricity. Contact areas (between the planet and its sun and outer ring gears), as well as the planet deflection, are functions of the independent parameters, defined as the planet thickness c, radius R, compressive force W, and the axial depth d. Axial depth has no effect on the optimization of planet size, since contact area varies linearly with d. For the example device, introduced in Section 1.3, an axial depth of 0.375 inches is used, and restrictions are imposed on the planet deflection δ, compressive force W, and thickness c. The restriction imposed on planet deflection is discussed with the results of the optimization in Subsection 3.1.4.

The compressive force W is chosen sufficiently low to limit wear and mechanical power loss due to friction. Frictional forces arise from the possible sliding between the rolling contact surfaces of the planet gear and the sun and ring gears. Still [1916] recommends that brushes in electric motors have a pressure of 1 or 2 pounds per square inch of the brush. This pressure produces a 1 to 2 pound compressive force on a one inch cross section brush. Since the sliding on the rolling contact surfaces of a flex-gear is much less than that of a brush, imposing a similar compressive force is conservative, in terms of limiting

wear and power loss. Hence, a compressive load of 3 pounds-force is imposed for the optimization of planet size of the example device.

A minimum planet thickness c is imposed to prevent excessive tooth deflection. Tooth deflection of a planet gear is exaggerated in Figure 3.3. The deflection of the foundation of a standard gear tooth can be found in numerous publications [such as Nakada and Utagawa, 1956]. However, none of the investigated publications take into account the radial thickness of a hollow gear or the thickness of a rack. The search for the minimum planet thickness to adequately limit tooth deflection is recommended for future study in Section 6.2. For the optimization of planet size in the example device, intuitively a minimum planet thickness of 0.04 inches is imposed.

The current-carrying capability of the device is restricted more by the contact between the planets and sun than the contact between the planets and the outer ring. This is intuitively evident, since contact area depends on the radii of curvatures at contact. As inferred from Figure 3.2, the radius of curvature of the sun is always less than that of the outer ring. The *planet contact area* is defined as the contact area between a planet and the sun, while the *total contact area* is defined as that of all the planets. Figure 3.4 shows part of a planet that is in contact with the sun, where the distance $2b$ denotes the contact length.

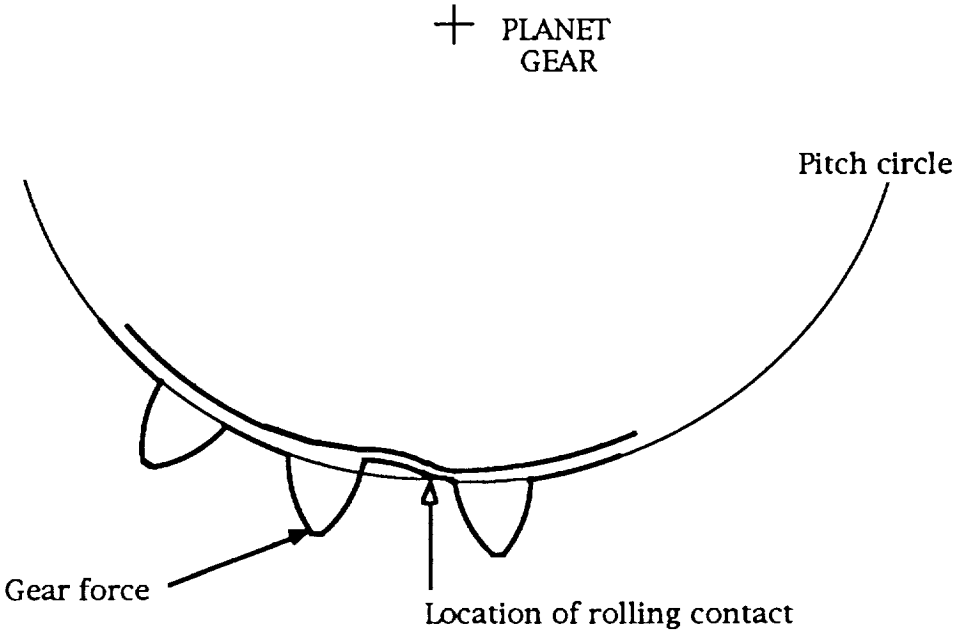

Figure 3.3: Tooth Deflection

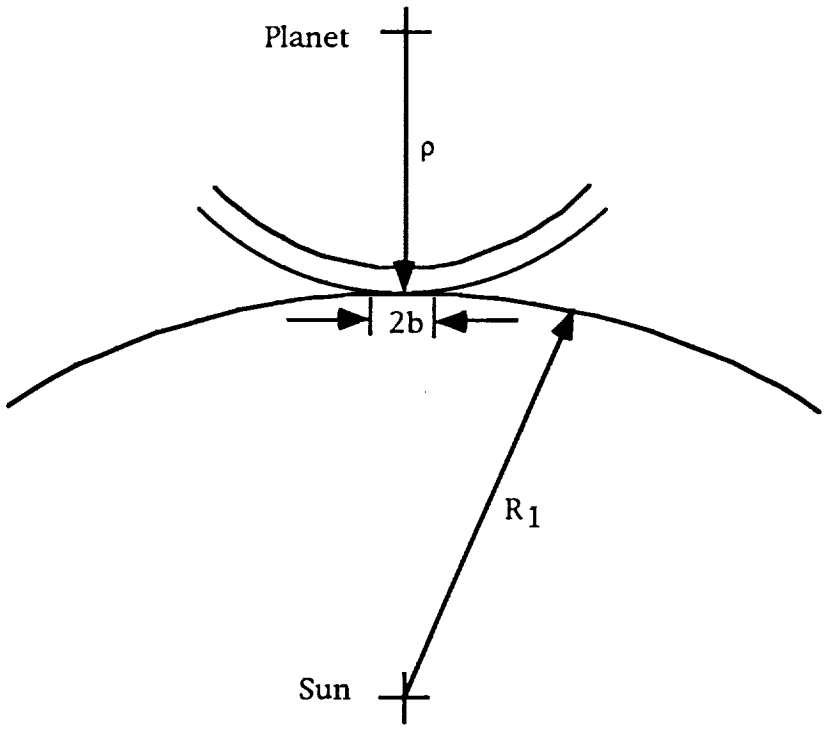

Figure 3.4: The Contact Region

Two models are used to determine the planet contact area and deflection. In Section 3.1, a closed-form model is developed, and its results are presented. In Section 3.2, a finite element model is developed, and its results are compared to those of the closed-form model.

3.1 Closed-form Model

Previously in this chapter, the electrical contact area between two spheres was said to be predicted by the Hertz contact theory because of high contact pressure. Here, it is further assumed that the electrical contact area between a flexible planet and its sun and outer rings also follows the Hertz contact theory because of high contact pressure. Such a planet is shown in Figure 3.1a with an exaggerated Hertzian pressure distribution. Hertz contact is a close approximation as long as the flexible planet does not globally flatten like the thinner ring shown in Figure 3.1b.

The Hertz contact theory was derived for two solid semi-infinite bodies in contact. Additional deformation of the planet, due to its hollowness, must be considered separately. Subsection 3.1.2 describes the deformation of the planet, which is referred to as *global deformation*. Subsection 3.1.3 describes the deformation of the contact region between the sun and the planet, which is referred to as *local deformation*.

3.1.1 Geometry

For geometric relationships, the planet deflection δ is assumed to be much less than the planet radius R, as shown in Figure 3.2b. Hence, the planets approximately maintain their circular shape, and the device radii are related by

$$R_3 = R_1 + 2R \tag{3.1}$$

For positive values of R_1 and an R_3 of approximately 3 inches (as given in Section 1.3 for the example device), the planet radius R can range from zero to 1.5 inches.

The number of planets that can fit in the annulus is a function of their radii R. As planet radius increases, the maximum possible number of planets n decreases. As shown in Figure 3.5, the angle that half of each planet consumes in the annulus is given by,

$$\gamma = \arcsin\left(\frac{R}{R_1 + R}\right) \tag{3.2}$$

By equating the angles of all the planets to 2π, the maximum number of planets can be found:

$$2\gamma n = 2\pi \tag{3.3}$$

Substituting Equation (3.2) into (3.3) and solving for n, yields

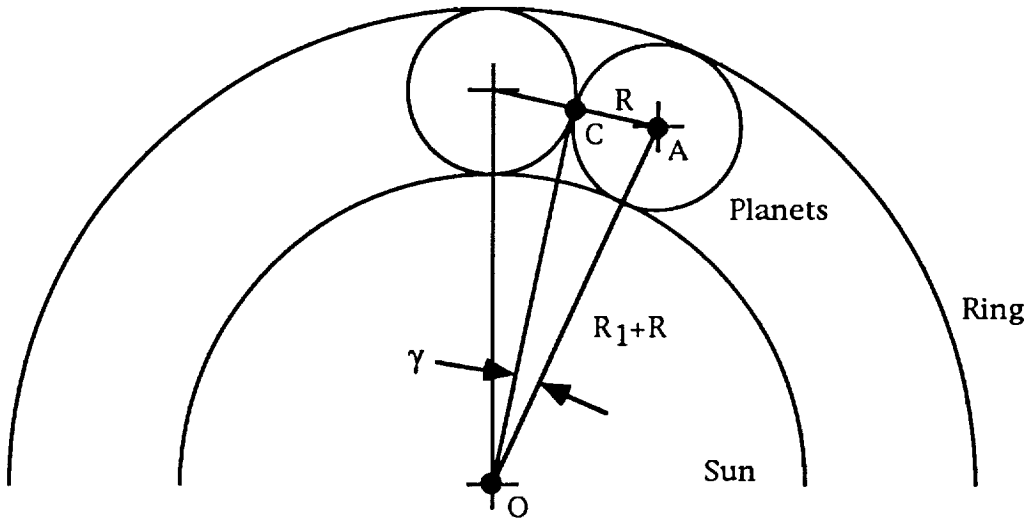

Figure 3.5: Maximum Number of Planets

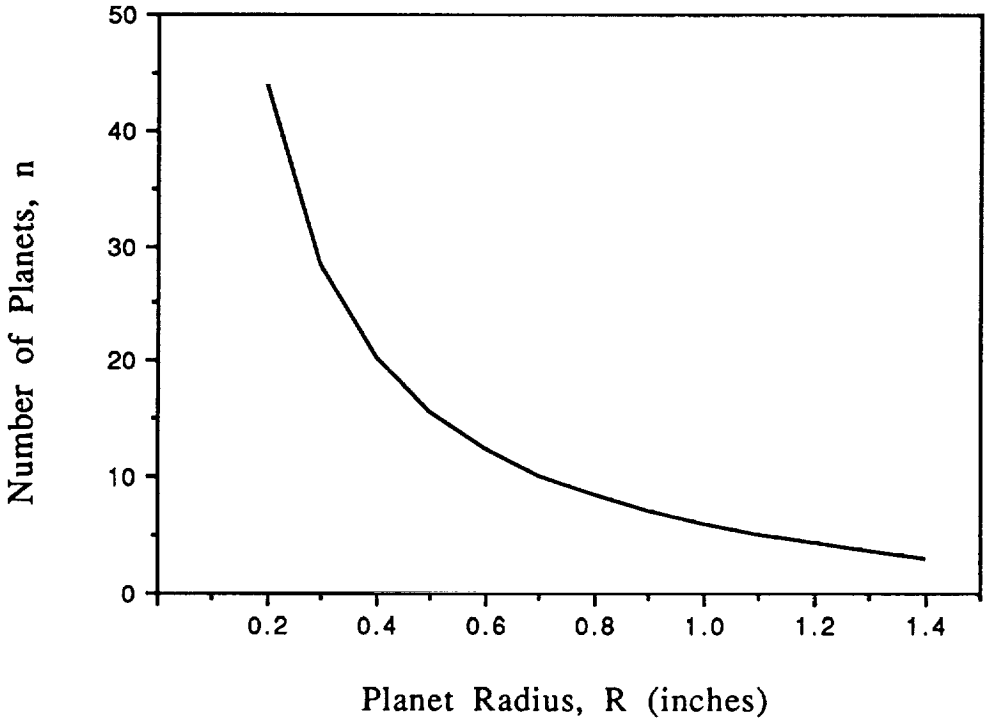

Figure 3.6: Number of Planets versus Planet Radius

$$n = \frac{\pi}{\arcsin\left(\frac{R}{R_1 + R}\right)} \qquad (3.4a)$$

Given R_3 equals 3 inches, this equation becomes

$$n = \frac{\pi}{\arcsin\left(\frac{R}{3 - R}\right)} \qquad (3.4b)$$

Equation (3.4b) is plotted in Figure 3.6 for realistic values of R.

3.1.2 Global Deformation

The total planet deflection δ, shown in Figure 3.2b, is the sum of the ring (or global) deformation and contact (or local) deformation. The global deformation of the planet is modeled by a ring diametrically compressed by two opposing point loads. The local deformation of the planet is modeled by the Hertz contact theory.

The *global planet deflection* δ_G is given by Timoshenko [1936] as a function of diametrical force W,

$$\delta_G = \frac{2WR^3}{EI}\left(\frac{\pi}{8} - \frac{1}{\pi}\right) \qquad (3.5)$$

where E is the elastic modulus and I is the area moment of inertia of the planet cross section about the x-x axis, as shown in Figure 3.7 ($I = d \cdot c^3/12$). As specified in Section 1.3, standard casting beryllium-copper alloy is used for the example flex-gear device.

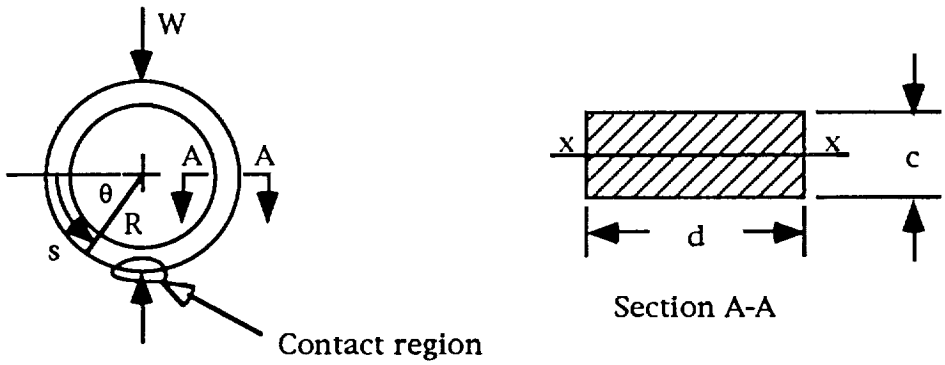

Figure 3.7: The Area Moment of Inertia of the Planet

According to the American Society for Metals [1978], the mechanical properties of standard casting beryllium-copper include $E=18.5\times10^6$ psi and $\nu=0.3$.

The curvature of the planet at the contact region affects the local deformation, which determines the contact area and local planet deflection (see Equation (3.12)). Timoshenko [1936] describes the curvature of a diametrically loaded ring as a function of θ:

$$\kappa(\theta)=\frac{1}{R}\left(1+\frac{\upsilon(\theta)}{R}\right)+\frac{d^2\upsilon(\theta)}{ds^2} \qquad (3.6)$$

where $\upsilon(\theta)$ is the radial deflection of the ring, and is given by,

$$\upsilon(\theta)=\frac{WR^3}{EI}\left(-\frac{1}{\pi}+\frac{\theta\cdot\sin\theta}{4}+\frac{\cos\theta}{4}\right) \qquad (3.7)$$

and s is the distance along the circumference from the horizontal of the planet, as shown in Figure 3.7. Substituting $s=\theta R$ into Equation (3.6) and simplifying, yields

$$\kappa(\theta)=\frac{1}{R}+\frac{1}{R^2}\left(\upsilon(\theta)+\frac{d^2\upsilon(\theta)}{d\theta^2}\right) \qquad (3.8)$$

Substituting the second derivative of the radial deflection with respect to θ into Equation (3.8), the curvature at the contact region ($\theta=\pi/2$) is found. The *radius of curvature* ρ is defined as the inverse of curvature κ at the contact region:

$$\rho = \frac{1}{\kappa|_{\theta=\pi/2}} = \frac{1}{\frac{1}{R} - \frac{RW}{\pi EI}} \tag{3.9}$$

The radius of curvature ρ is used in the next subsection to find the deformation local to the contact region.

3.1.3 Local Deformation

As shown in Figure 3.4, the *semi-width contact length* b is defined as one half of the length of contact along the circumference of the planet. By the Hertz contact theory, the semi-width contact length between the sun and planet is given by

$$b = \sqrt{\frac{2W\Delta}{\pi d}} \tag{3.10a}$$

where Δ is given by,

$$\Delta = \frac{\left(\frac{1-\nu_1^2}{E_1} + \frac{1-\nu_2^2}{E_2}\right)}{\frac{1}{2R_1} + \frac{1}{2\rho}} = \frac{\left(\frac{1-\nu_1^2}{E_1} + \frac{1-\nu_2^2}{E_2}\right)}{\frac{1}{2(R_3 - 2R)} + \frac{1}{2\rho}} \tag{3.10b}$$

where ν is Poisson's ratio, and the subscripts *1* and *2* refer to the sun and planet, respectively.

The contact area between each planet and the sun is called the *planet contact area* and is given by

$$A_i = 2bd \qquad (3.11a)$$

The contact area between all the planets and the sun is called the *total contact area* and is given by

$$A_t = nA_i \qquad (3.11b)$$

Contact area is used in the next section to determine optimal planet size.

The *local planet deflection* δ_L is found from the Hertz contact theory [Stolarski, 1990].

$$\delta_L = \frac{2W(1-\nu^2)}{\pi d E}\left[\ln\left(\frac{4R_1}{b}\right)+\ln\left(\frac{4\rho}{b}\right)-1\right] \qquad (3.12)$$

Comparing Equations (3.12) and (3.5), the local planet deflection δ_L is much less than the global planet deflection δ_G (for a *thin ring*, which is defined by a ring, whose radius is over ten times its radial thickness). Because the optimum planet is assumed to be a thin ring, the local planet deflection δ_L is neglected. Hence, the total planet deflection δ is given by the global planet deflection δ_G, in Equation (3.5).

3.1.4 Optimization

The planet contact area A_i, defined in Equation (3.11), is a function of the planet thickness c and radius R, for a given

compressive force W and axial length d. This function is plotted in Figure 3.8. The planet contact area initially increases with increasing planet radius R, because the decreasing planet curvature improves contact. Further increasing the planet radius decreases the planet contact area, because the decreasing sun curvature degrades contact. Decreasing the planet thickness c slightly increases the planet contact area by further decreasing the curvature of the planet at contact. However, as can be seen from Figure 3.8, the effect of planet thickness on contact area is small.

The total contact area A_t, as defined in Equation (3.11b), is plotted with respect to planet radius R, in Figure 3.9. The shape of this curve is very similar to the shape of the curve for the number of planets in Figure 3.6, but not to the shape of the curve for the planet contact area, in Figure 3.8. This indicates that the number of planets plays a dominant role in the determination of total contact area. Hence, the maximum contact area follows the maximum number of planets. The number of planets is increased simply by decreasing the planet radius. However, decreasing planet radius also decreases planet deflection, which has a minimum determined by machining tolerances.

The effect of machining errors on planet deflection can be seen from the equation of planet deflection:

$$\delta = (R_3 - R_1) - 2R \qquad (3.13)$$

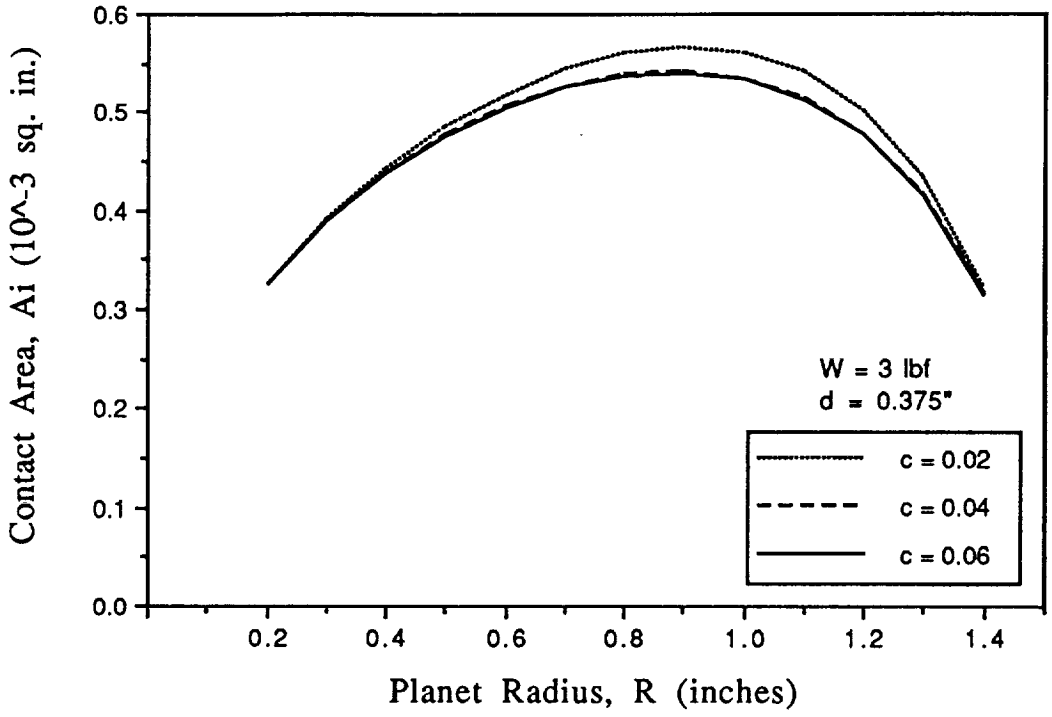

Figure 3.8: Planet Contact Area versus Planet Radius

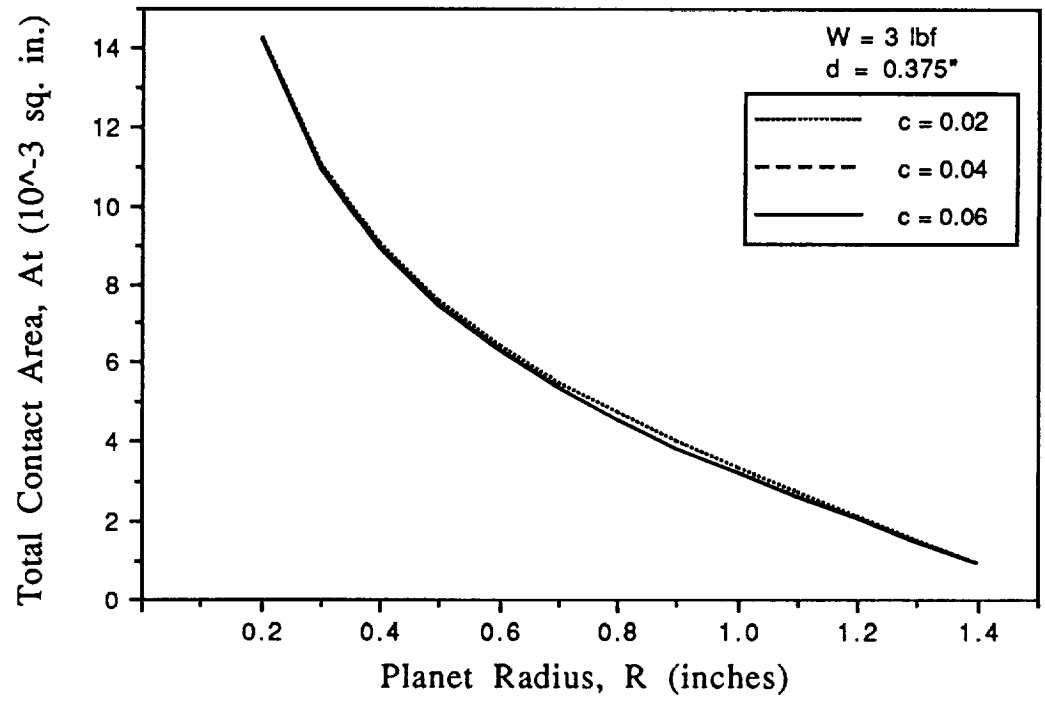

Figure 3.9: Total Contact Area versus Planet Radius

where R_1 and R_3 are the sun and outer ring gear radii, respectively. By Equation (3.13), a unilateral machining tolerance of 0.001 inches on all gear radii allows, at most, a variance of planet deflection of 0.004 inches. Requiring at least some contact at all times, the smallest planet deflection is zero and the largest, defined as the nominal deflection, is 0.004 inches. To insure contact at all times, the minimum nominal deflection equals the variance of the planet deflection. For the example device, unilateral tolerances of 0.001 inches are used, yielding a minimum nominal deflection of 0.004 inches.

Figure 3.10 shows the deflection δ as a function of the radius R and thickness c, for a compressive force of $W=3$ lbf and axial depth of $d=0.375$ inches. The minimum planet deflection, set forth by machining tolerances, is indicated in Figure 3.10 by the horizontal line at $\delta=0.004"$. The smallest planet radius, which yields the largest total contact area, occurs at the minimum planet deflection and the smallest recommended planet thickness $c=0.04"$. The resulting planet radius of 0.7 inches yields a planet contact area of 0.00073 square inches, by Figure 3.8, and a maximum number of 9 planet gears, by Figure 3.6. The product of these values yields a total contact area of 0.0066 square inches, as alternatively taken from Figure 3.9.

The closed-form model of the optimization of planet gear size is compared to a finite element model in the following section.

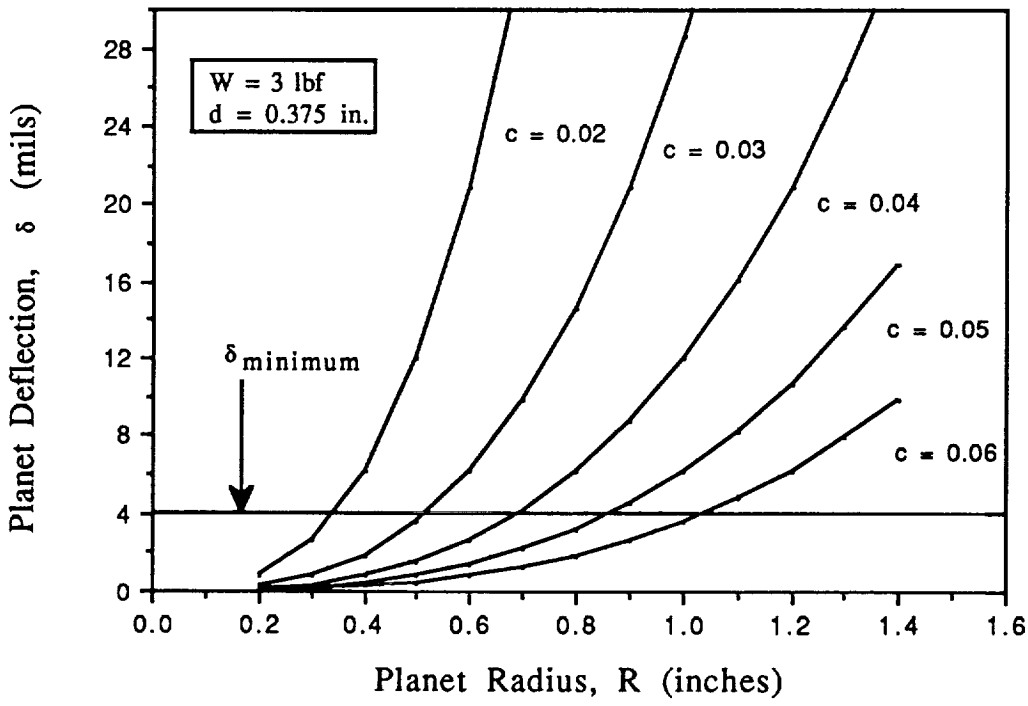

Figure 3.10: Planet Deflection versus Planet Radius

3.2 Finite Element Model

The finite element model is shown in Figure 3.11. The compressive force W is applied as a point load far from the contact region, as shown in Figure 3.11a. Only the contact region between the sun and the planet was modeled, since this contact limits the current-carrying capability of the device.

To model the sun and planet, 4-node plane strain quadrilateral elements were used. Figure 3.11b shows how gap elements were used to model the contact region. Gap elements and their ability to model this contact problem is discussed in the following subsection.

3.2.1 Contact Modeling

The contact area is allowed to increase non-linearly with the compressive force. The finite element package ABAQUS does this by applying the compressive force incrementally. Each gap element has no effect on the model unless the nodes that define its endpoints pass each other in the vertical direction. If this occurs, the two nodes are constrained together in that direction. Once the entire compressive force has been applied, the closed gap elements indicate the contact area. The distance between the closed gap elements that are farthest apart is twice the semi-width contact length. This times the axial length of the planet d equals the contact area.

Gap elements are placed between the planet and sun, as shown in Figure 3.11, inside the suspected contact region. This

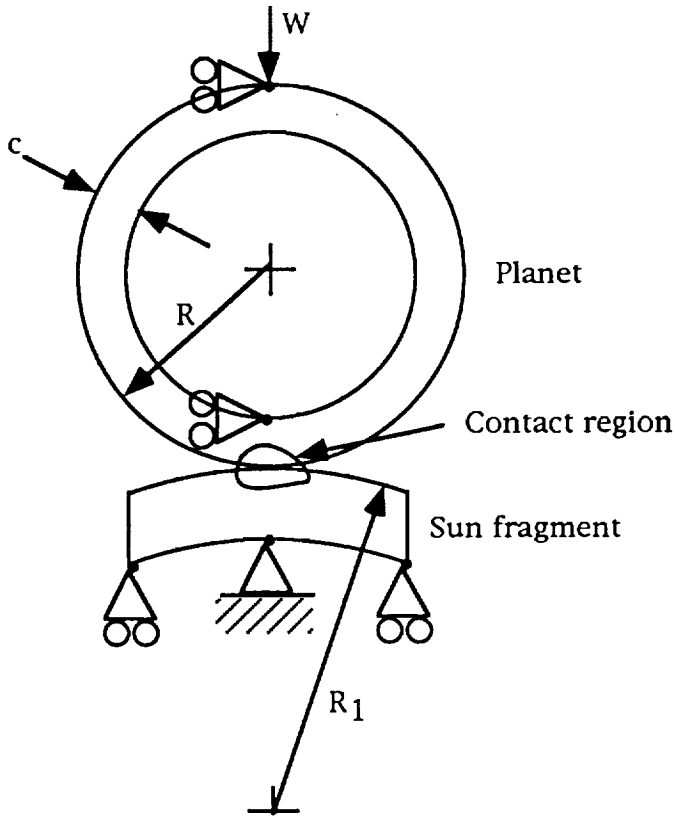

(a) Global Modeling

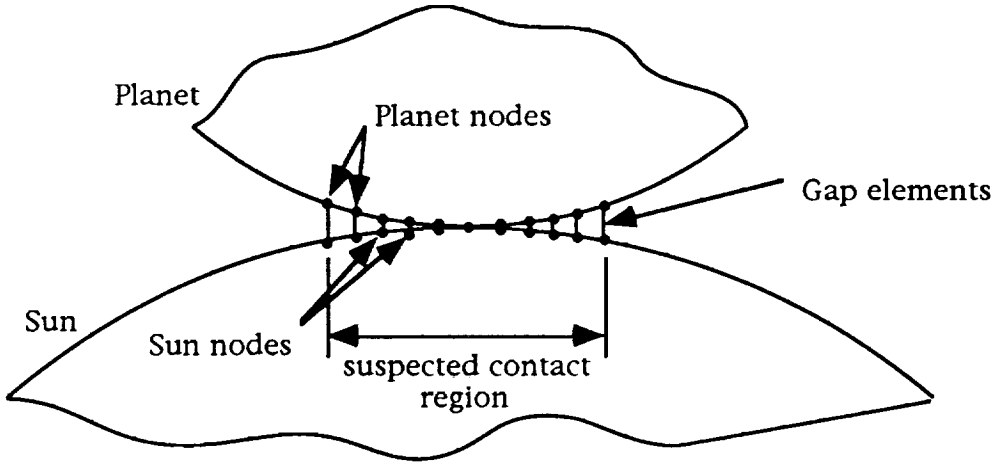

(b) Contact Modeling

Figure 3.11: Finite Element Model of Flexible Planet

region spans approximately three times the contact distance that is predicted by the closed-form solution.

To build confidence in the use of gap elements to model a contact region, the solution of contact area of a finite element model with gap elements is compared to that of the corresponding Hertz model. Two solid cylinder fragments in compression, as shown in Figure 3.12, were modeled by finite elements. The solutions of contact area and y-normal stress along the x and y axes are compared to the Hertz solutions in Figures 3.13a and b, respectively. Overall, the finite element solution agrees with the Hertz solution. However, the contact area of the finite element solution is 12% less than the Hertz solution.

The stress along the y-axis matches the Hertz solution more closely than at contact. This is because the points along the y-axis are further from the contact area, where reaction forces occur. The finite element results along the y-axis deviate slightly from the Hertz solution near the contact point for the same reason. Increasing the density of the gap and quadrilateral elements is expected to yield results that agree with the Hertz contact theory more closely.

The agreement of the finite element solution with the Hertz contact theory builds confidence in the modeling of the contact region by gap elements. To apply gap element modeling to the contact between a flexible planet and its sun, the proper density of the gap and quadrilateral elements are determined through refinements of the gap and quadrilateral meshes.

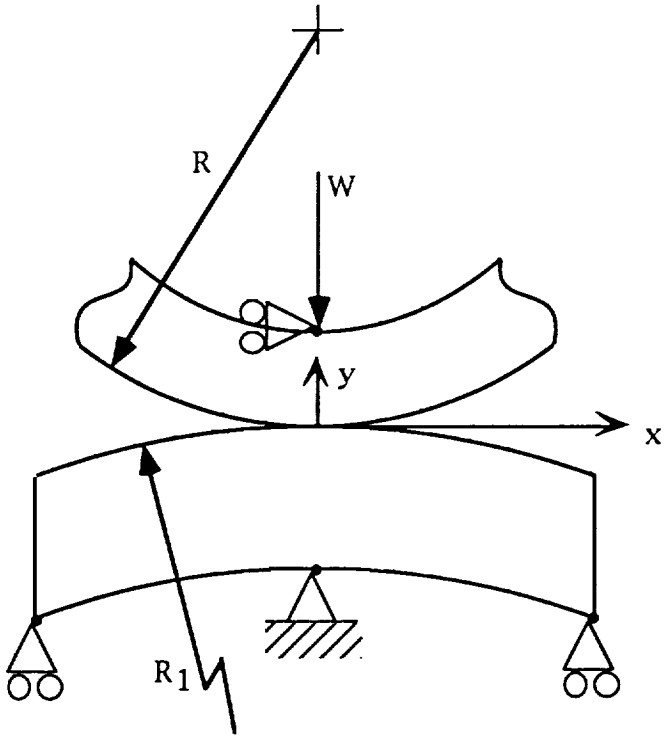

Figure 3.12: Finite Element Model of Two Cylinder Fragments

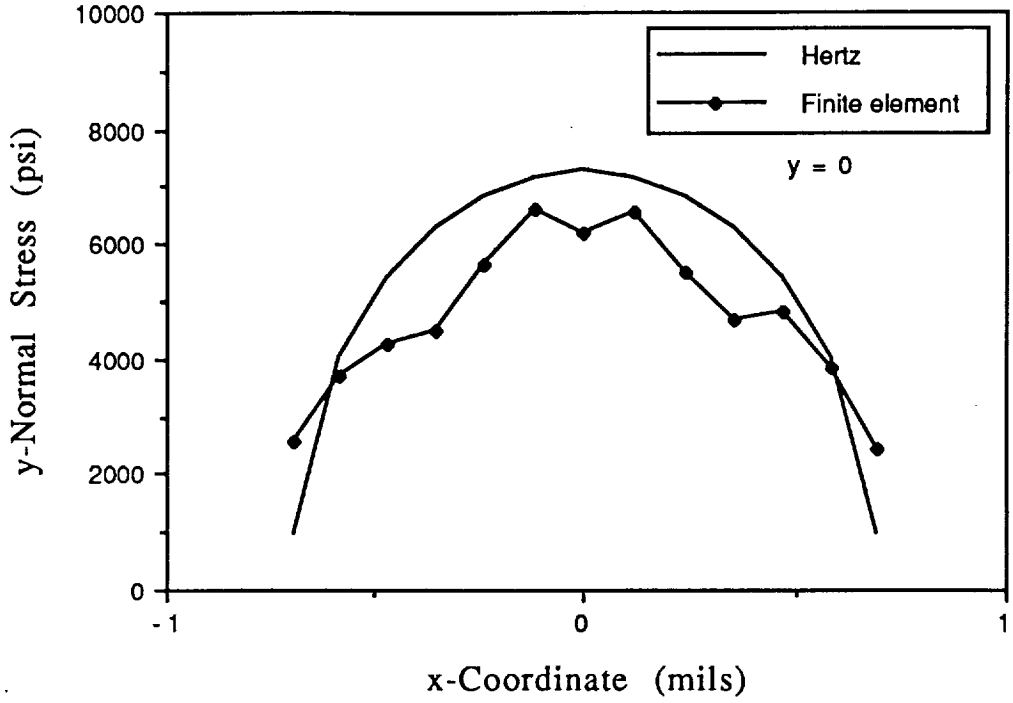

(a) Stress at Contact

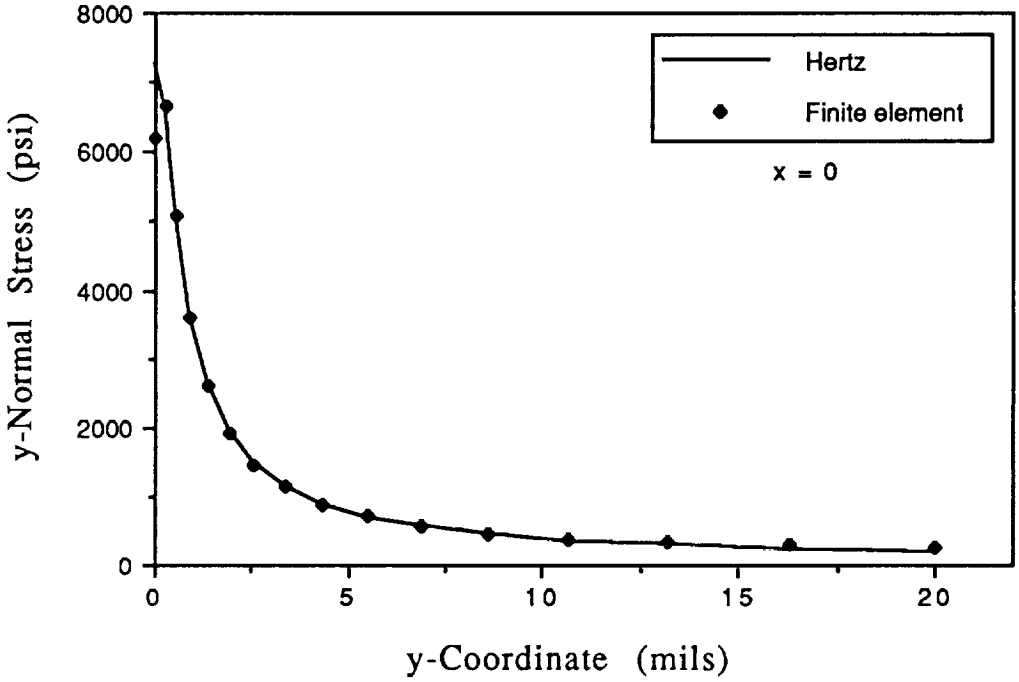

(b) Stress along the y-axis

Figure 3.13: Stress of Solid Cylinder Fragments in Contact

3.2.2 Mesh Refinements

To insure a suitable density of gap and quadrilateral elements for model accuracy, three mesh refinements were performed. The first was performed on the *pinned-ring model* shown in Figure 3.14. This suggested a suitable quadrilateral mesh density in the planet to accurately predict its global deflection. The second and third mesh refinements were performed on the *planet model* shown in Figure 3.11. The second refinement indicated a sufficient density of gap elements to accurately predict the contact area. With the density of gap elements determined in the second mesh refinement, a final mesh refinement was performed on the planet model to insure that the planet mesh from the first refinement was sufficiently dense to accurately predict the deflection of the planet (as opposed to the pinned ring used in the first mesh refinement). Also checked in the final mesh refinement was the effect of the planet mesh on the solution of contact area.

The results of the first mesh refinement, performed on the pinned ring, are shown in Figure 3.15. There is little difference in the solution of deflection, especially between the 300 and 480 element meshes. Either mesh is acceptable for an accurate solution of diametrical deflection. However, the 300 element mesh takes significantly less time to run than the 480 element mesh, and is therefore used initially in the planet model.

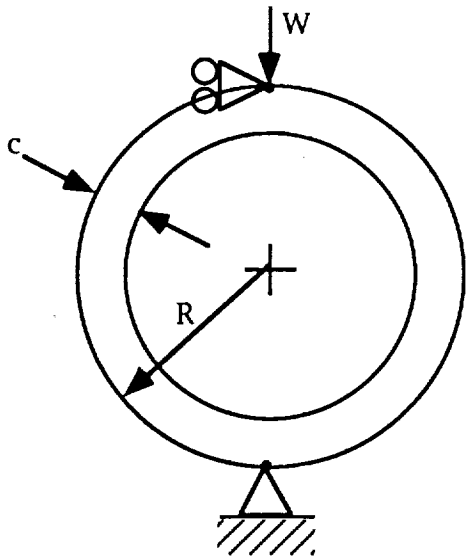

Figure 3.14 Finite Element Model of a Pinned Ring

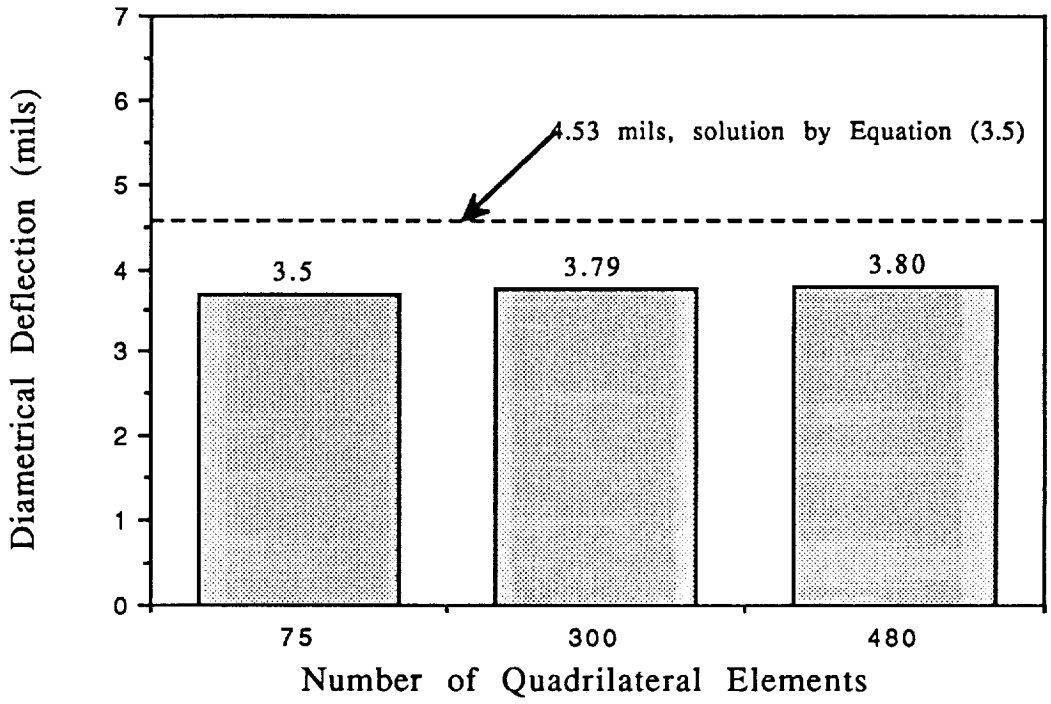

Figure 3.15: Mesh Refinement of the Pinned Planet

The deflection of the pinned ring model is simply the global deflection of the planet, which is predicted by Equation (3.5). The solution of global deflection by this equation is shown in Figure 3.15. The finite element solutions, given in this figure, are about 16% less than this.

The second mesh refinement compares the solution of contact area for three different densities of gap elements. The higher the density of gap elements, the more accurate the solution of contact area is expected to be. Figure 3.16 shows the solutions of contact area for each of the gap element densities. As the number of gap elements increases, the model appears to asymptotically approach a specific solution. A density of 27 gap elements in the contact region is gauged to predict this solution with sufficient accuracy.

After adding 27 gap elements to the planet model, a final mesh refinement was performed to insure that the 300-element planet mesh, determined by the first mesh refinement, maintains an accurate prediction of the planet deflection and contact area. The solution of contact area is identical for all the tested planet meshes. Figure 3.17 shows that planet deflection changes very little with an increasing number of planet elements. There is little difference between the results of especially the 300 and 400 element meshes. As in the first mesh refinement, the 300 element mesh takes considerably less time to run. To curb the time to complete the optimization without much loss of

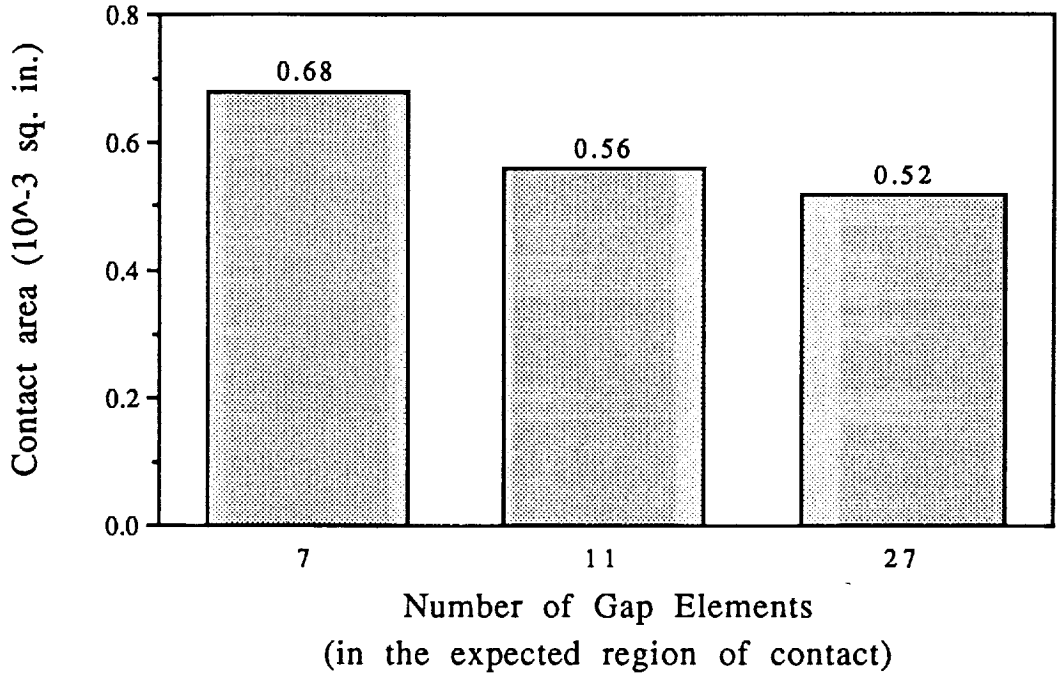

Figure 3.16: Gap Element Mesh Refinement

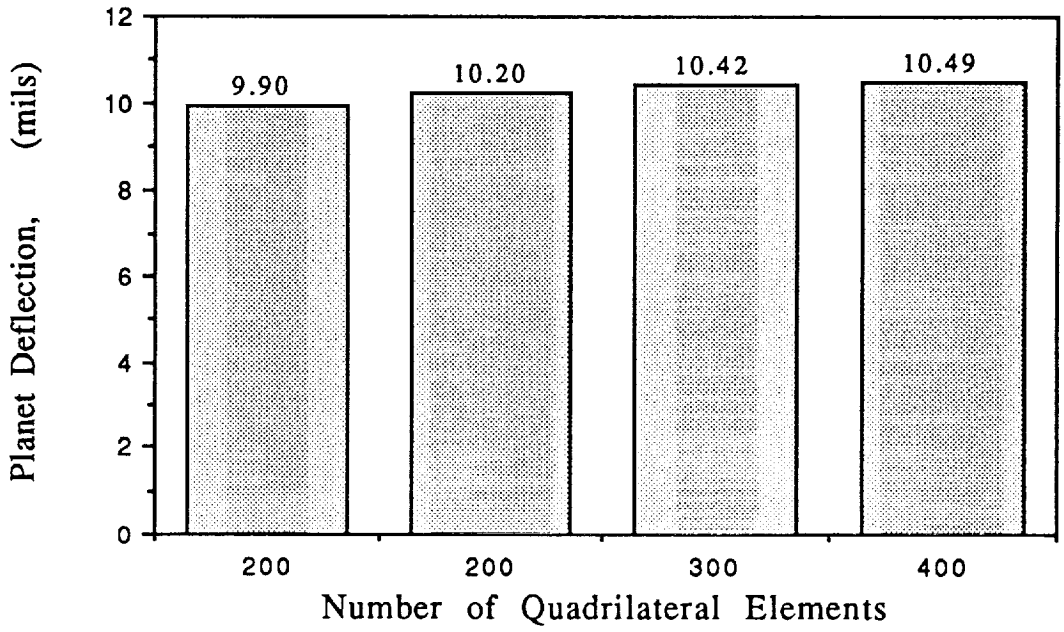

Figure 3.17: Planet Mesh Refinement

accuracy, the 300-element planet mesh was chosen for the planet model.

In summary, the best planet model, in terms of efficiency versus accuracy, consists of approximately 300 quadrilateral elements in the planet and 27 gap elements at contact. Near the contact region, the quadrilateral elements are more dense to maintain connectivity with the densely positioned gap elements. Similarly, the mesh of the sun fragment is sufficiently dense.

3.2.3 Optimization

The results of the finite element optimization are compared to the closed-form optimization in Figures 3.18 and 3.19. The overall results of both planet deflection and contact area concur. However, the finite element solutions for total deflection are consistently about 15% less than those of the closed-form solution. This is approximately the same as the difference of the global deflections in the mesh refinement of the pinned ring. This implies that the local radial deflection δ_L is indeed much smaller than the global radial deflection δ_G, thereby supporting the closed-form solution in its dismissal of the local radial deflection δ_L, in Subsection 3.1.3.

In Subsection 3.1.4, the optimum size of the planets with respect to their rolling contact surfaces were found. The resulting flex-gear device is shown in Figure 3.20. In Chapter 4, the addition of gear teeth will be considered.

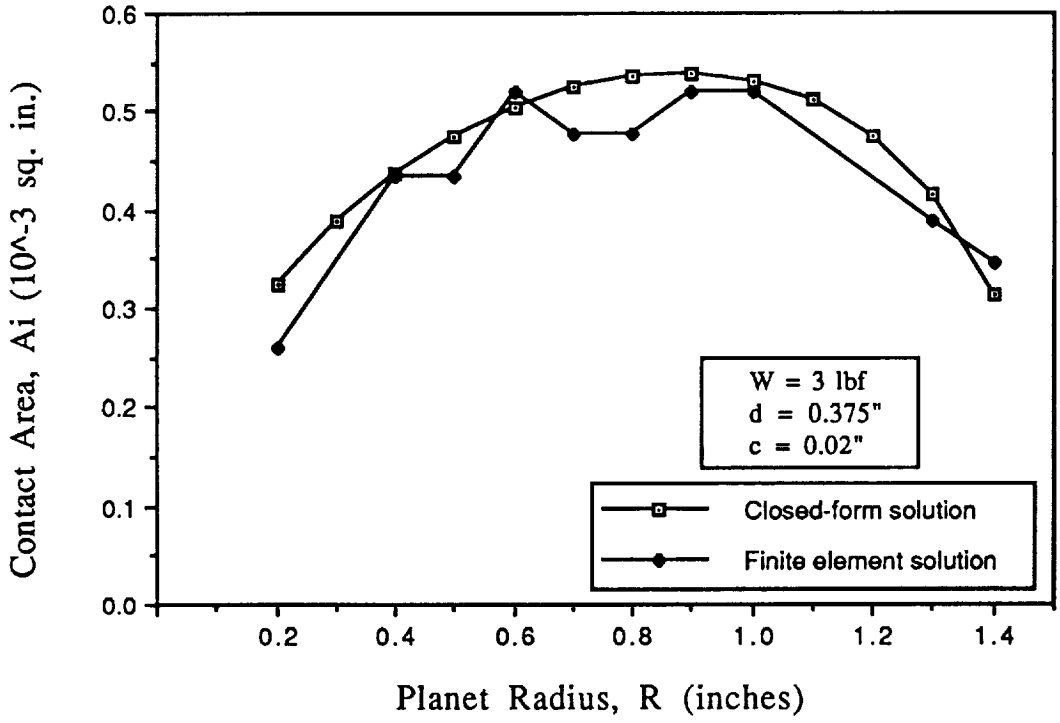

Figure 3.18: Comparison of Finite Element and Closed-form Solutions of Planet Contact Area

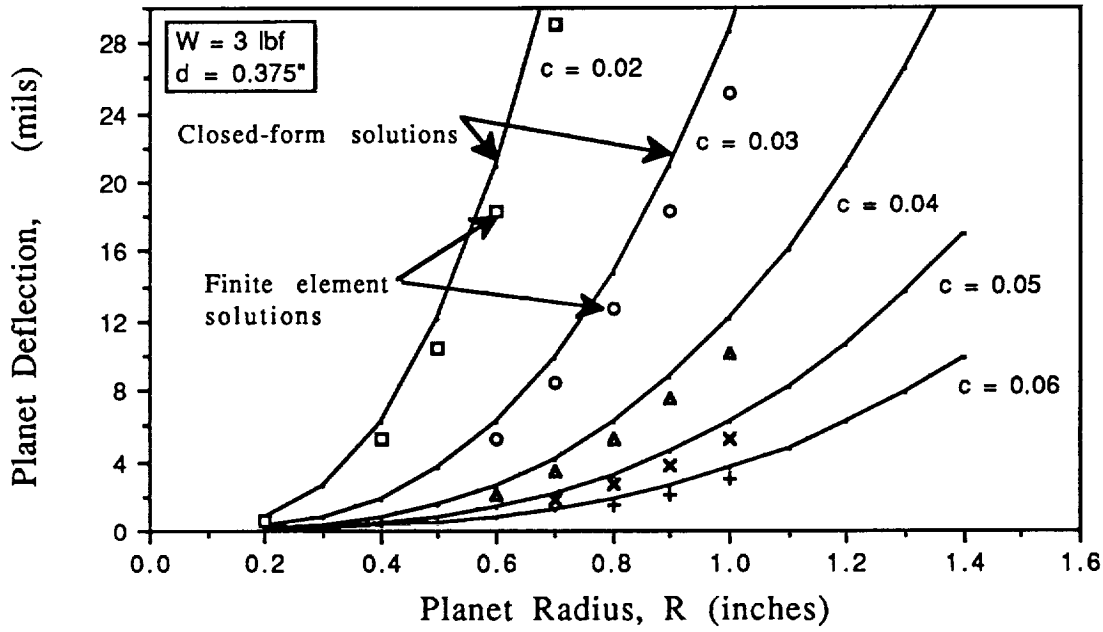

Figure 3.19: Comparison of Finite Element and Closed-form Solutions of Planet Deflection

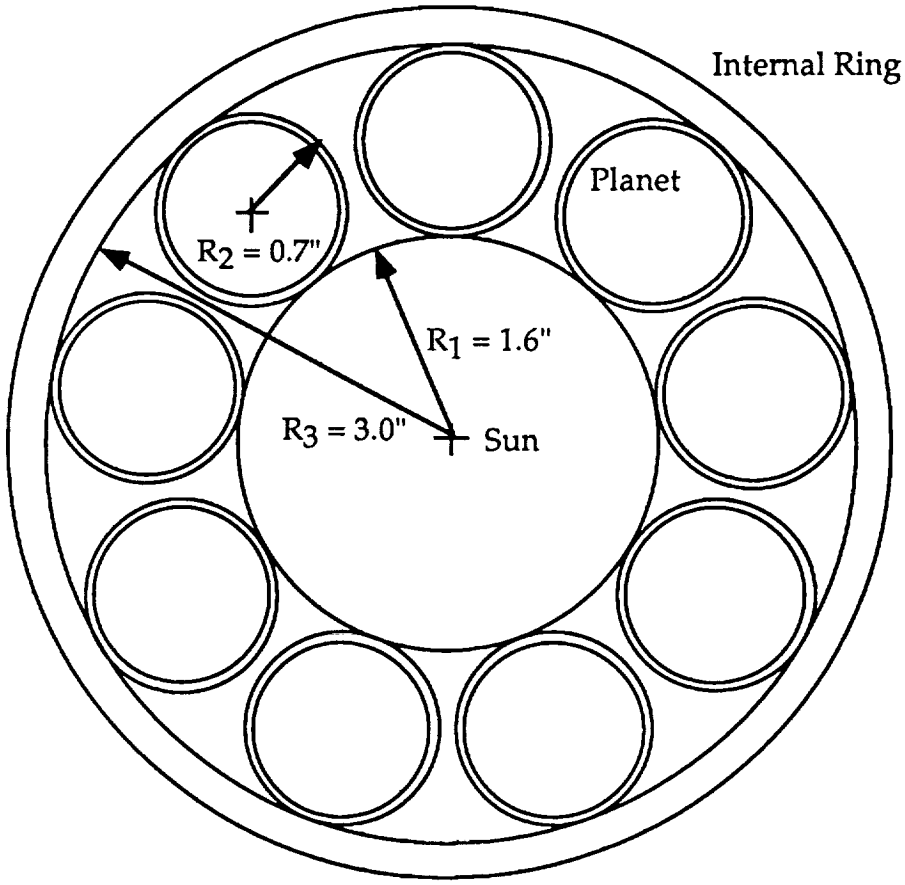

Figure 3.20: Optimum Dimensions of the Example Device

CHAPTER 4

DESIGN OF GEAR TEETH

In the preceding chapter, gear teeth were neglected for the optimization of planet size. In this chapter, the addition of teeth is considered. Adding gear teeth lessens the duration of contact between the rolling surfaces of pitch-rolling-gears. In Section 4.1, the teeth of the planet gear are sized for a minimum loss of rolling contact surface. Section 4.2 investigates the properties of pitch-rolling-gears and their application to flex-gear devices.

4.1 Tooth Size

From Chapter 2, the preferred configuration of a planetary flex-gear device has addendum gear teeth on the planet gear, and corresponding dedendum gear teeth on the sun and ring gears. To maintain a high current-carrying capability, the planet gear

teeth are sized such that the duration of contact between the rolling surfaces of the gears is maximized.

Pitch-rolling-gear teeth are shown in Figure 4.1. A contact ratio, as defined by Equation (2.1), near 1.0 promotes a high duration of contact between rolling surfaces by spacing the teeth as far apart as possible. This contact ratio is depicted in Figure 4.1, where tooth *1* initiates contact with the dedendum gear at point *A*, at the same time as tooth *2* ends contact at point *P*. A contact ratio of 1.0 is used in the optimization of tooth size to maximize the duration of contact between rolling contact surfaces. The contact ratio will be slightly increased after the optimization of tooth size to prevent the catastrophe of tooth skipping.

Addendum tooth dimensions are shown in Figure 4.2. The height of the tooth or the addendum is given by a. The *angle of tooth action* α is the gear rotation through which each mating pair of involute gearing surfaces are in contact. The distance y is the length of the line of action and is measured along the pressure line. The tooth thickness t, pitch p, and the arc of tooth action q are measured along the pitch circle. The arc length i is the length of the projection of the side of the tooth onto the pitch circle. The thickness of the tooth at the addendum circle is called the *addendum tooth thickness* t_a. A minimum addendum tooth thickness is required to limit the shear stress induced by the gear force at point *A*, shown in Figure 4.1. An addendum tooth

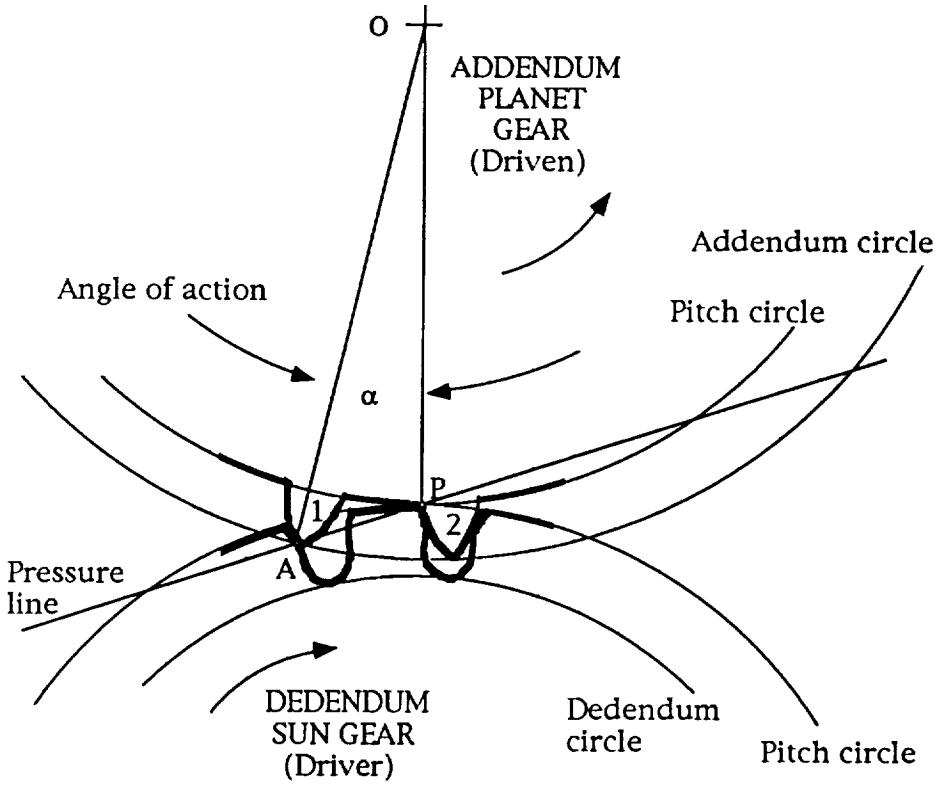

Figure 4.1: Pitch-rolling-gear Teeth

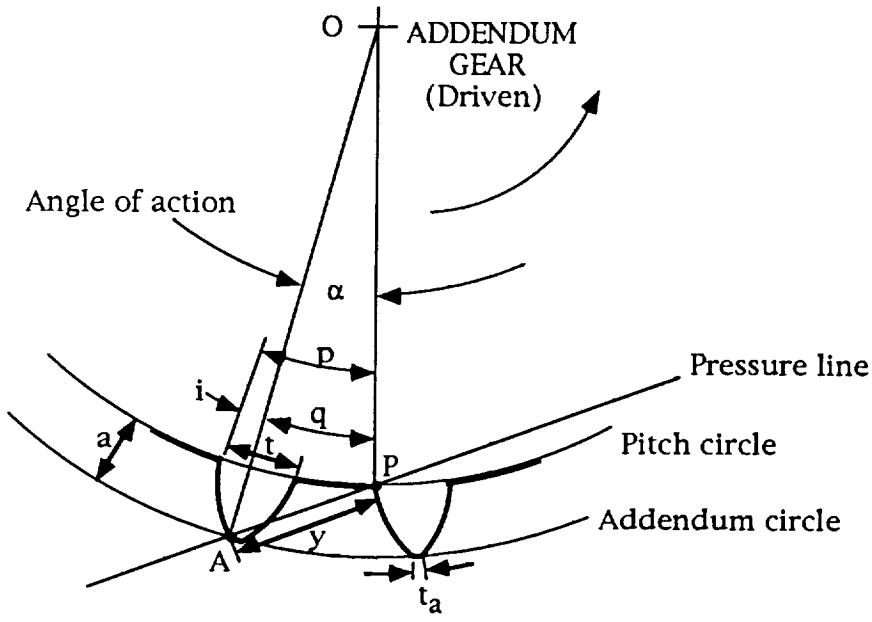

Figure 4.2: Nomenclature of an Addendum Gear

thickness of 0.003 inches is used for the optimization of tooth size. The resulting shear stress is checked in Section 5.1.4.

The *duration of contact* λ is defined as the ratio of the rolling surface of a planet gear to that of a toothless planet. The length of the rolling surface of a toothless planet is equal to its circumference. The same size planet gear has a total rolling surface equal to its circumference minus the sum of the thickness of its teeth. So, the duration of contact is

$$\lambda = \frac{2\pi R - Nt}{2\pi R} = \frac{\frac{2\pi R}{N} - t}{\frac{2\pi R}{N}} \qquad (4.1)$$

where N is the number of teeth on the planet gear. The *pitch* of a gear is defined as the distance between teeth along the pitch circle. Since the pitch circle has a radius R,

$$p = \frac{2\pi R}{N} \qquad (4.2)$$

Substituting Equation (4.2) into (4.1),

$$\lambda = \frac{p - t}{p} = 1 - \frac{t}{p} \qquad (4.3)$$

All the tooth dimensions that are shown in Figure 4.2 are functions of tooth height a, for a given planet radius R, contact ratio cr, pressure angle ϕ, and addendum tooth thickness t_a. In

this section, the relationships between the dimensions in Figure 4.2 are defined, and the duration of contact λ is solved with respect to tooth height a.

The tooth thickness t along the pitch circle is related to the addendum tooth thickness t_a by the shape of the involute curve [Kimbrell, 1991]:

$$t = 2R\left(\frac{t_a}{2R_a} - \text{inv}\phi + \text{inv}\phi_a\right) \tag{4.4}$$

where the *addendum radius* $R_a = R + a$. The angle ϕ_a is given in Kimbrell [1991] as

$$\phi_a = \arccos\left(\frac{R}{R_a}\cos\phi\right) \tag{4.5}$$

and $\text{inv}\phi$ is defined by $\text{inv}\phi = \tan\phi - \phi$. A standard pressure angle of $\phi = 20^\circ$ will be used for the optimization of tooth size, for the example device.

According to Figure 4.2, the pitch p is given by

$$p = q + i \tag{4.6}$$

where the arc length i equals half the tooth thickness when $t_a = 0$. So, by Equation (4.4),

$$i = \frac{1}{2}t\Big|_{t_a=0} = R(\text{inv}\phi_a - \text{inv}\phi) \tag{4.7}$$

The arc length q is given by

$$q = \alpha R \tag{4.8}$$

The angle of action α is found from the triangle OAP, in Figure 4.3. Applying the law of cosines to the angle α,

$$\alpha = \arccos\left(-\frac{y^2 - R_a^2 - R^2}{2R_a R}\right) \tag{4.9a}$$

where y, the length of the line of action, is found by applying the law of cosines to the angle β in triangle OAP of Figure 4.3:

$$y^2 - (2R\cos\beta)y + (R^2 - R_a^2) = 0 \tag{4.9b}$$

where $\beta = \phi + \pi/2$. The possible solutions of y are given by

$$y = R\cos\beta + \frac{1}{2}\sqrt{4R^2\cos^2\beta - 4\left(R^2 - R_a^2\right)} \tag{4.9c}$$

Substituting the resulting angle of action α into Equation (4.8), then (4.8) and (4.7) into (4.6), the pitch p is solved as a function of gear radius R, pressure angle ϕ, and tooth height a. Substituting this pitch and the tooth thickness t, from Equation (4.4), into Equation (4.3), the duration of contact λ is solved with respect to R, ϕ, and a. The resulting equation for the duration of contact is a long transcendental equation. This

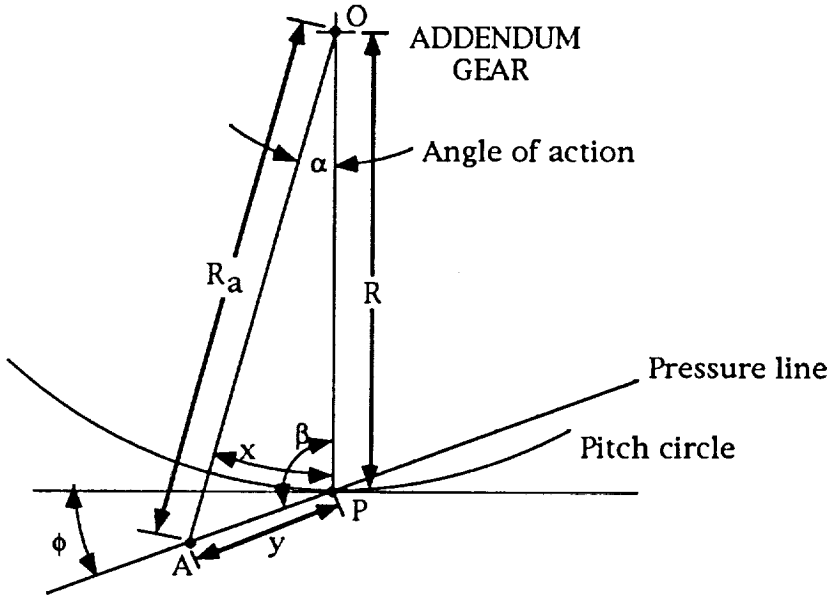

Figure 4.3: The Angle of Action

equation is plotted in Figure 4.4, for the planet gear radius $R=0.7"$, chosen in Chapter 3, and a standard pressure angle of $\phi=20°$.

For extremely small tooth heights, the duration of contact is low because the tops of the gear teeth reduce contact. As gear tooth height increases, this effect is diminished because the pitch p, increasing to maintain a contact ratio of 1.0, increases the duration of contact by Equation (4.3). The maximum duration of contact occurs at a tooth height of approximately 0.022 inches. By further increasing the tooth height a, tooth thickness t increases by Equations (4.4) and (4.5), thereby decreasing the duration of contact by Equation (4.3). The duration of contact decreases slowly past maximum to only 7% less than maximum at a tooth height of 0.06 inches. Accordingly, a gear tooth height of 0.025 inches is chosen. This is a reasonable size, since standard gear teeth of 48 diametral pitch* have an addendum of 0.0208 inches [Boston Gear, 1985].

When the valleys of the dedendum gear straddle the addendum teeth of the mating gear, rolling contact is hindered. Referring to Figure 4.5a, robust electrical contact occurs before contact reaches point A. As the planet rotates to the position shown in Figure 4.5b, the sun gear, whose teeth are not shown, straddles the planet tooth with poor contact at points A and B. The resulting momentary loss of robust electrical contact is

* The diametral pitch of a gear equals its number of teeth divided by its pitch diameter in inches. Diametral pitch alone determines the size of standard gear teeth.

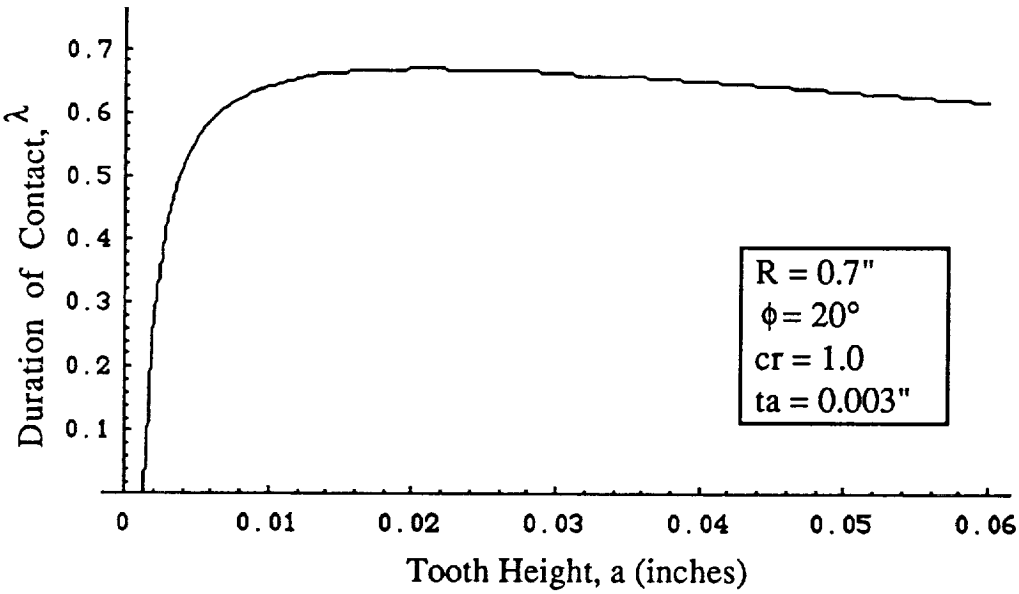

Figure 4.4: Duration of Contact versus Tooth Height

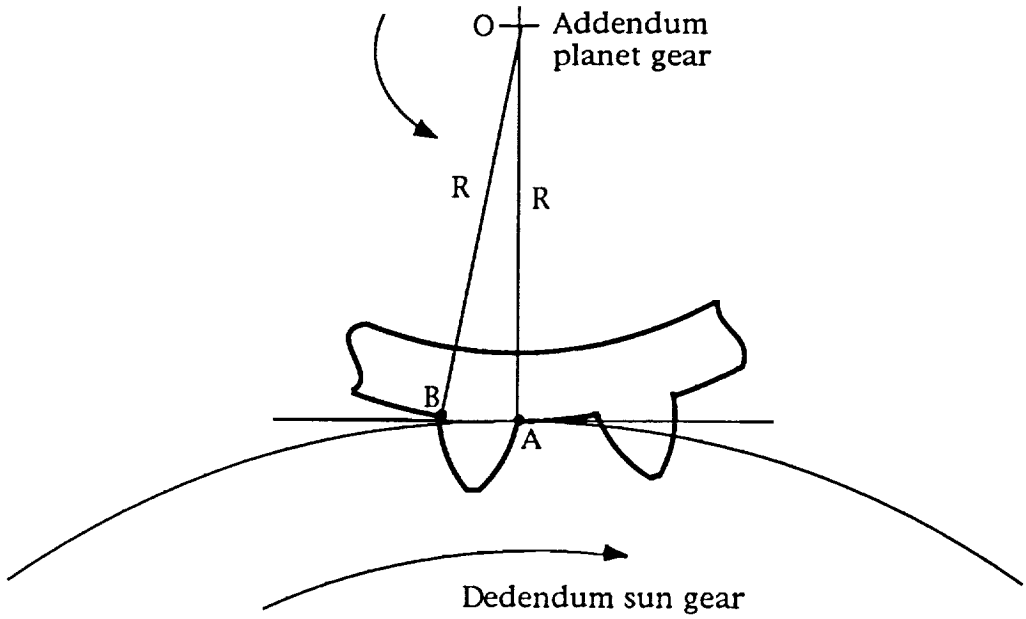

(a) Rolling Contact

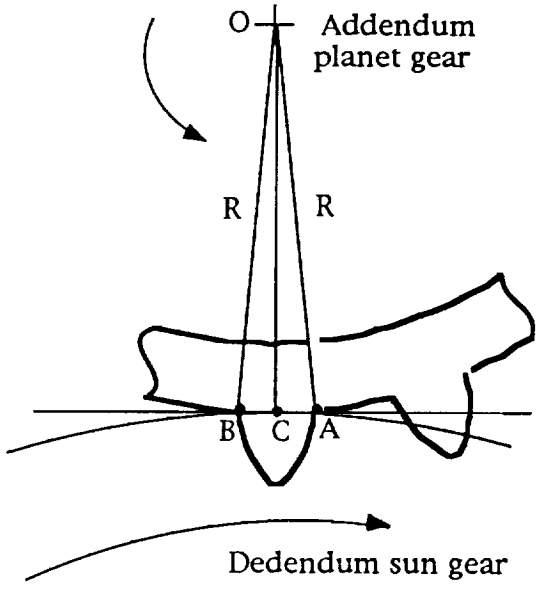

(b) Tooth Straddle

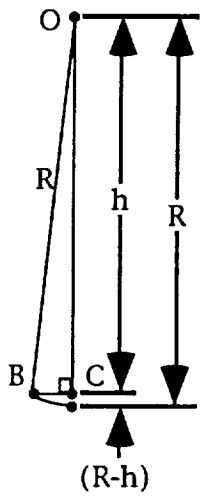

(c)

Figure 4.5: Tooth Straddle

compensated by the other planet gears in the flex-gear device. Another result of tooth straddling is that the distance between the centers of the sun and planet gears is decreased, momentarily hindering conjugate action. By the right triangle BOC, shown in Figure 4.5c, the center distance lost from the planet gear is given by

$$h_p = \sqrt{R^2 - \left(\frac{t}{2}\right)^2} \qquad (4.10a)$$

Similarly, the center distance lost from the sun gear, for the example device, is given by

$$h_s = \sqrt{R_1^2 - \left(\frac{t}{2}\right)^2} = \sqrt{(3-2R)^2 - \left(\frac{t}{2}\right)^2} \qquad (4.10b)$$

The resulting change in the center distance between the sun and planet gears is $h = h_p + h_s$. For a tooth thickness of 0.023 inches (corresponding to a tooth height of 0.025 inches of the example device), h equals 0.0002 inches. Since this is much less than the center distance between the sun and planet gears, its effect on conjugate gear action is negligible.

All gear specifications are determined by the tooth height a as portrayed in Figure 4.4, given the planet gear radius R, pressure angle ϕ, addendum tooth thickness t_a, and contact ratio cr. Using a gear tooth height of 0.025 inches, gear specifications for the example device are calculated and shown in Table 4.1.

Tooth size: a=0.025", t=0.023", R=0.70"			
N	64	70	80
p	0.0687"	0.0628"	0.0550"
cr	1.014	1.109	1.267
λ	0.661	0.629	0.576

Table 4.1: Tooth Specifications of the Example Device

Here, the contact ratio cr is no longer constrained to 1.0 for two reasons. Foremost, the number of planet gear teeth N must be constrained to integer values. Furthermore, a slightly higher contact ratio is sought to safeguard against the catastrophe of tooth skipping. The tooth size is held constant ($a=0.025"$, $t=0.023"$), while the number of teeth N is varied.

A planet gear with 70 teeth is chosen because it has a reasonable contact ratio cr of 1.1 and a duration of contact λ within 5% of maximum. The design of the planet gear for maximum current-carrying capability is now complete. The optimum planet for the example device is shown in Figure 4.6. The application of this planet gear to flex-gear devices is considered in the following section.

4.2 Pitch-rolling-gear Flex-gear Devices

With the design of the planet gear complete, the corresponding sun and outer ring gears must be chosen. If the sun and outer ring gears are chosen such that the planet gear fits perfectly in the annulus of its sun and ring gears, the planet deflection is zero and gear meshing follows Chapter 2. However, to maintain robust electrical contact, the rolling contact surfaces of the planet must be compressed by the deflection δ in the annulus of the sun and ring gear, in accordance with Chapter 3.

Consider the flex-gear device shown in Figure 3.2, where the lines depict rolling contact surfaces. In Chapter 2, the rolling contact surfaces of pitch-rolling-gears were positioned exactly

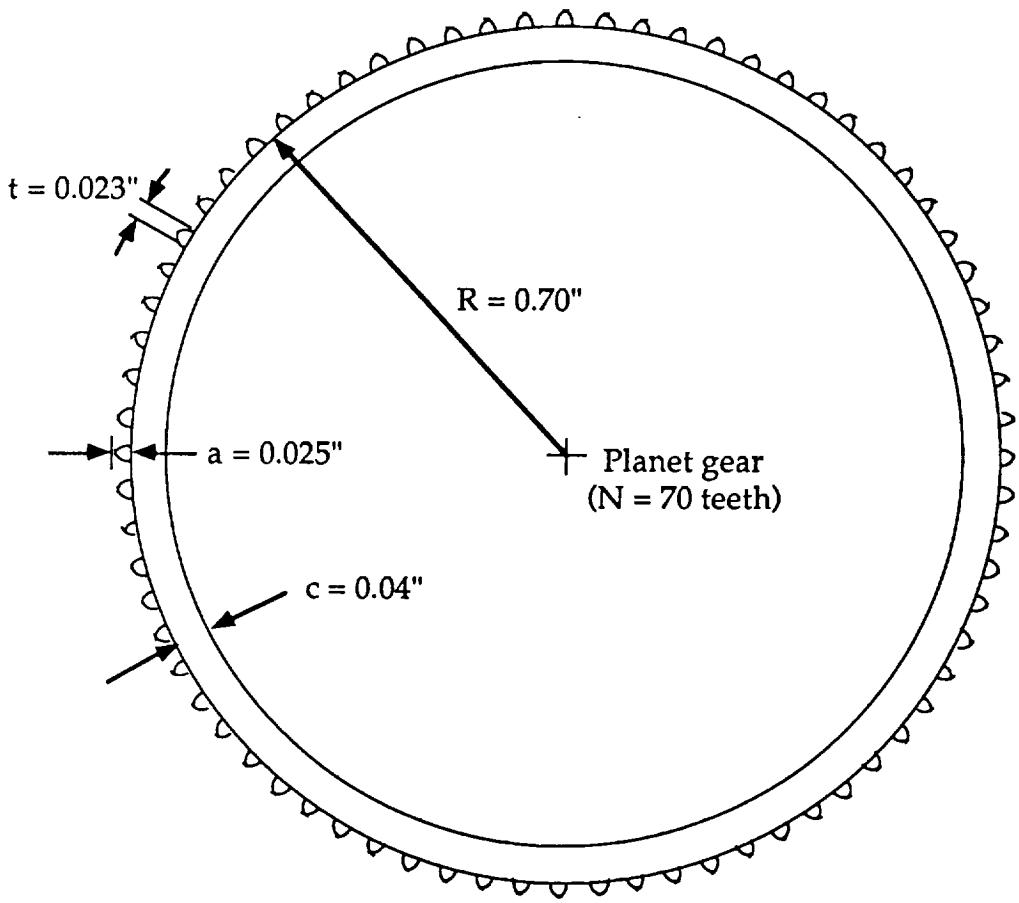

(a) Dimensions (3:1 scale)

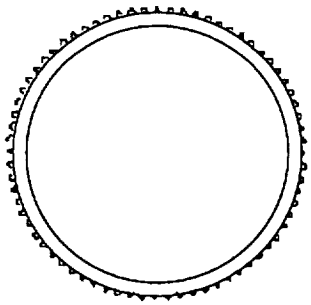

(b) Actual Size

Figure 4.6: Optimum Planet Gear for the Example Device

on the pitch circles for pure rolling. However, this is not always possible, as will be shown. The pitch circle of a gear was defined in Chapter 2 as having a radius that purely rolls on the pitch circle of the mating gear. The *contact circle* of a pitch-rolling-gear is defined as having a radius that indicates the location of the rolling contact surfaces. The difference between the pitch and contact circles is distinguished in Figure 4.7.

Pitch, defined previously in Equation (4.2) as the distance between gear teeth along the pitch circle, is redefined here with the *pitch radius* r, and is henceforth referred to as the *gear pitch* p.

$$p = \frac{2\pi r}{N} \tag{4.11a}$$

Contact pitch p_c is defined as the distance between teeth along the contact circle, i.e.,

$$p_c = \frac{2\pi R}{N} \tag{4.11b}$$

where R denotes the *contact radius*. Unless otherwise stated, the contact and pitch circles are coincident, so that their radii are equal.

First, consider a flex-gear device with no planet gear compression. Planet compression, required for robust electrical contact, is produced by oversizing the contact radius of the planet or sun gear, or undersizing that of the outer ring gear.

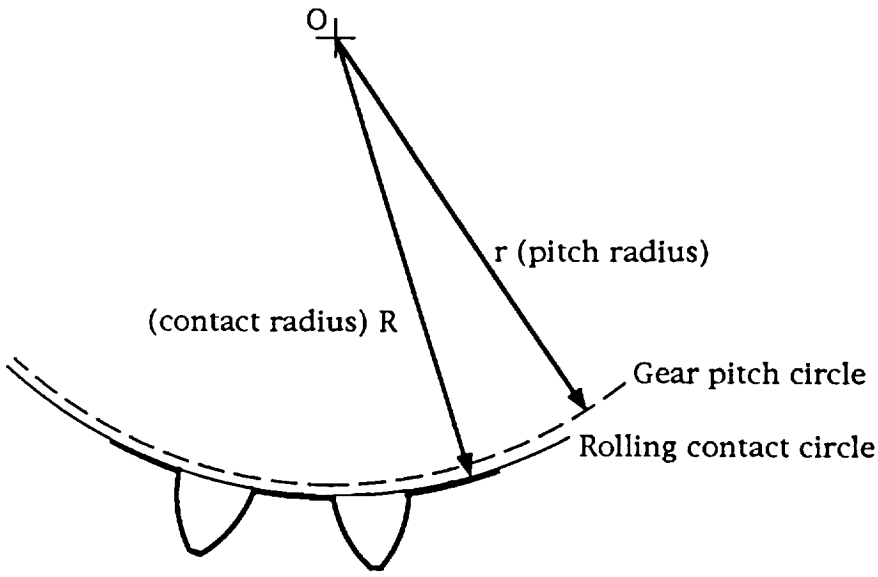

Figure 4.7: Contact and Pitch Circles

Both the resizing of contact radii and the resulting planet compression affect gear meshing in their own way. The change of the contact radii and the compression of a pitch-rolling-gear pair are considered separately in the following subsections.

4.2.1 Compressing a Pitch-rolling-gear

Consider the uncompressed gear *2* meshing with gear *1* in Figure 4.8. By design, the pitch circles coincide with the contact circles for pure rolling. Thus, the pitch point P, at the intersection of the pitch circles, coincides with the contact point A, at the intersection of the contact circles.

Developed in Chapter 2, uncompressed pitch-rolling-gears are simply a special case of standard gears. Therefore, the equations that govern their motion are the same. Standard gear pitch p is defined as the distance between teeth along the pitch circle:

$$p_1 = \frac{2\pi r_1}{N_1} \tag{4.12a}$$

$$p_2 = \frac{2\pi r_2}{N_2} \tag{4.12b}$$

where N_1 and N_2 are the number of teeth on the sun and planet gears, respectively. By definition, the pitches at the pitch point are equal, i.e.,

$$p = p_1 = p_2 \tag{4.13}$$

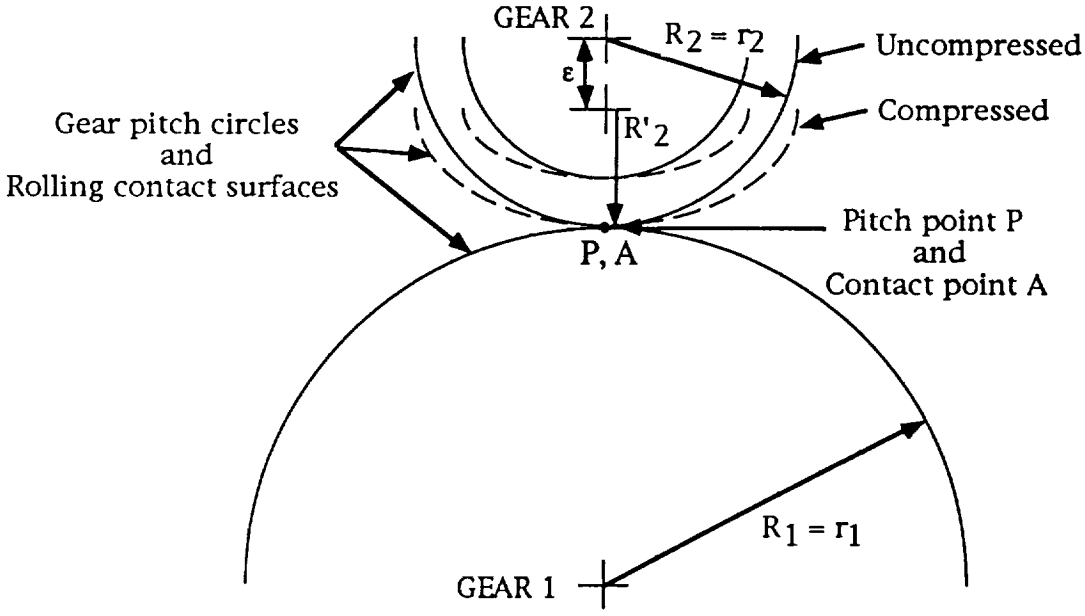

Figure 4.8: Compressing Pitch-rolling-gears

Likewise, the velocities of the two gears at that point are equal, i.e.,

$$\omega_1 r_1 = -\omega_2 r_2 \qquad (4.14)$$

And lastly, the sum of the pitch radii are confined by the center distance C, between gears *1* and *2*:

$$C = r_1 + r_2 \qquad (4.15)$$

Equations (4.12) through (4.15) are standard gear equations, which apply to uncompressed pitch-rolling-gears.

Now, consider compressing gear *2*, as shown in Figure 4.8, so that the contact radius changes by a distance ε, from R_2 to R_2'. Through compression, the angle and location of the gear forces between mating gearing surfaces change. However, since the desired compression of the gear, as recommended in Chapter 3, is over 100 times smaller than the gears, the pressure line, along which the gear forces act, is assumed to remain the same throughout compression.

Through gear compression, pure conjugate action is lost, since involute gear meshing is designed for circular gears. Without conjugate action, the velocity of the rolling contact surfaces of the mating gears at the point of contact is not the same. However, the *average* velocity of the gears at the contact point must be the same, since the contact pitch of both gears

remains the same throughout compression. The contact pitch of gear *2* remains the same throughout compression because the circumference of the contact circle of gear *2* does not significantly change. This supposition is supported by Timoshenko [1936], who used the inextensibility of thin rings to analyze their behavior under compression.

Defining the pitch point as the point of *average* rolling between meshing gears, the pitch point remains coincident with the contact point. Then, the equations that govern compressed pitch-rolling-gear meshing are similar to those of uncompressed pitch-rolling-gear meshing (or standard gears). Through compression, Equations (4.12) and (4.13) apply to compressed gear meshing. However, Equation (4.15) becomes

$$C' = r_1 + r_2' = r_1 + (r_2 - \varepsilon) \tag{4.16}$$

and Equation (4.14) becomes

$$\omega_1 r_1 = -\omega_2' r_2' = -\omega_2'(r_2 - \varepsilon) \tag{4.17}$$

where ω_2' is the angular velocity of the planet gear, defined at the contact point A (at the compressed radius r_2'). Elsewhere on the planet gear, ω_2' is only the approximate angular velocity, since gear *2* is not a rigid body. The relationship between the angular velocity of compressed pitch-rolling-gears, as given by Equation

(4.17), is used in Chapter 5 in the kinematic analysis of an example flex-gear device.

At the beginning of this section, the pitch and contact points were said to be coincident before compression, so that no sliding occurred on the rolling contact surfaces. By the same argument, compression has no effect on the final location of the pitch point with respect to the contact point, regardless of the initial locations of the contact and pitch points. Thus, the magnitude of sliding remains the same throughout compression.

In summary, the contact and pitch points change negligibly by compressing pitch-rolling-gears together, whereas, the relative angular velocity ω_2'/ω_1 changes significantly. Before applying pitch-rolling-gears to flex-gear devices, the effect of changing the contact radius of a pitch-rolling-gear on gear meshing must be investigated.

4.2.2 Changing the Contact Radius

According to Equation (4.11b), there are two options upon resizing the contact radius R of a pitch-rolling-gear. One way to resize the contact radius is to maintain the same contact pitch p_c, forcing an increase in the number of teeth N. The second way to resize the contact radius is to maintain the same number of teeth, thereby forcing the contact pitch to increase. These options are considered in this subsection by changing only one gear of a pitch-rolling-gear pair, and allowing no compression of either

gear. Compression was considered separately in the previous subsection.

The first option, changing the number of teeth, maintains pure rolling on the rolling contact surfaces, because the contact and pitch circles remain coincident. However, the contact radius R, in Equation (4.11), can hold values only for which N is an integer. So, changing the number of teeth on a pitch-rolling-gear restricts the possible contact radii to discrete values.

The second option, holding the number of teeth N constant, increases the contact pitch p_c. Increasing the contact pitch of one gear, while holding that of the mating gear constant, produces some sliding between the contact circles (or rolling contact surfaces), because the contact and pitch circles of the modified gear are no longer coincident. Consider oversizing the contact radius of gear *2* by ΔC, as shown in Figure 4.9, without changing the number of teeth. Figure 4.9a shows an ideal gear pair, wherein the pitch point and the contact point coincide. Figure 4.9b shows the gear pair after oversizing the contact circle of gear *1*, where gear *2* is allowed to move up so that no compression occurs. Because the *gear pitch circles* that govern gear meshing are no longer in contact, they no longer act as the pitch circles. New pitch circles, called *working pitch circles*, pass through the *working pitch point* P, as shown in Figure 4.9b. The effect of oversizing the contact radius R is simply to increase the center distance of the gear pair.

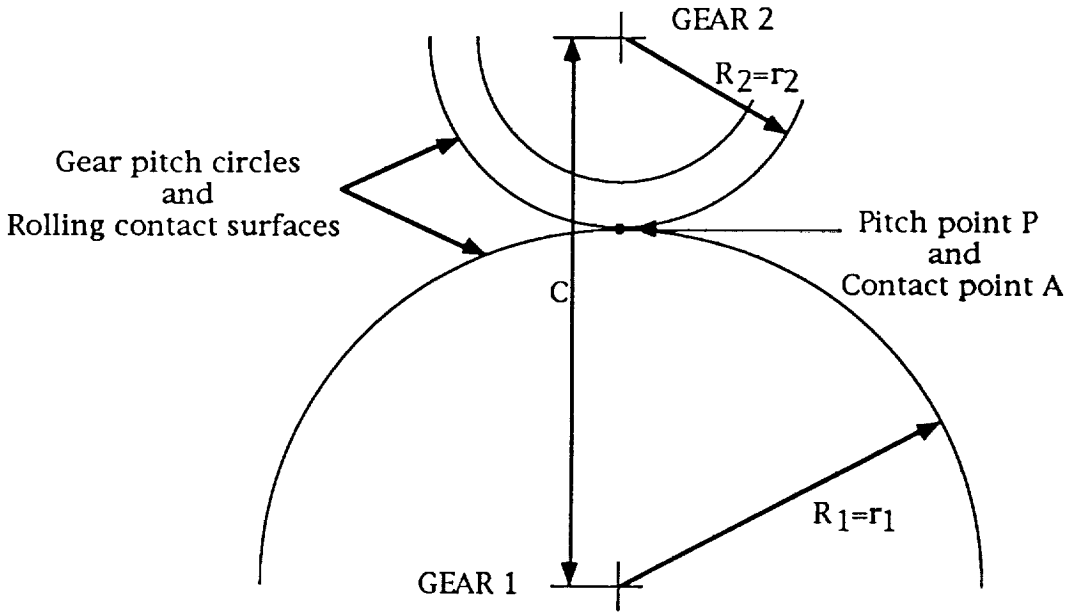

(a) Ideal Contact Radius

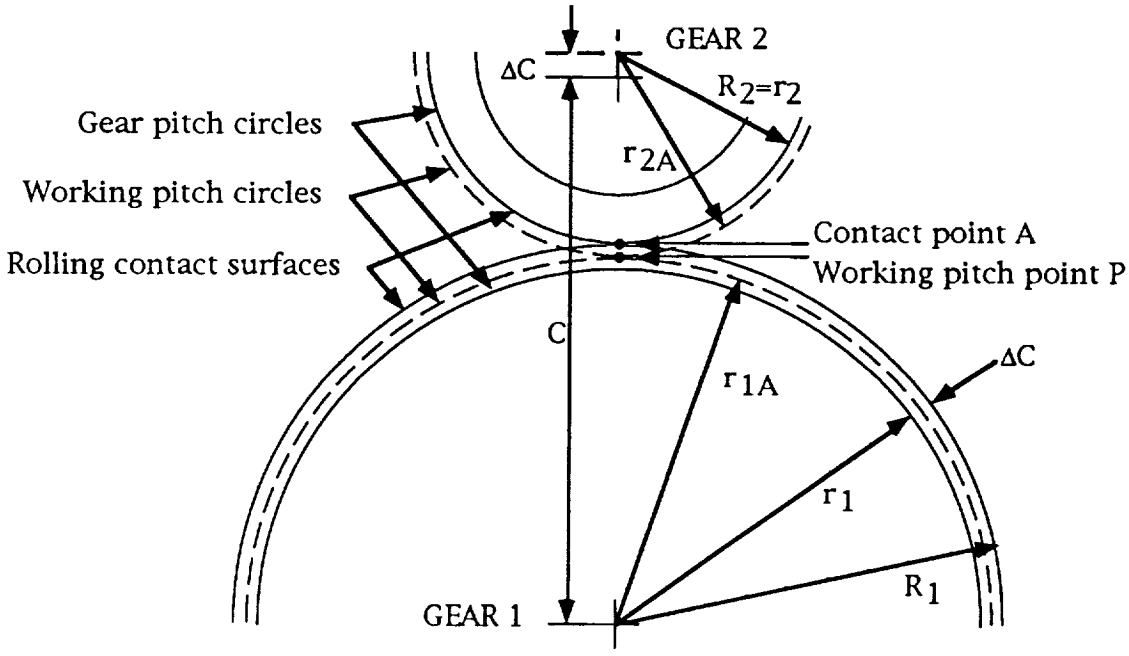

(b) Oversized Contact Radius

Figure 4.9 Changing the Contact Radius of Pitch-rolling-gears

Since pitch-rolling-gears are a special form of standard gears, the effect of their change in center distance is the same as that of standard gears. The effect of the change in center distance between standard gear pairs has been investigated to understand the effect of imperfectly mounted gears, from errors in machining and assembly. Since the number of teeth remains the same, the relative angular velocity between the gear pair remains the same. From this, the location of the working pitch point P is found [Kimbrell, 1991]. The corresponding working pitch radii r_{1A} and r_{2A} are given by

$$r_{1A} = \frac{N_1}{N_1 + N_2}(C + \Delta C) \qquad (4.18a)$$

$$r_{2A} = \frac{N_2}{N_1 + N_2}(C + \Delta C) \qquad (4.18b)$$

where ΔC is the change in center distance C between gears. The working pressure angle is given by Kimbrell [1991] as

$$\phi_A = \arccos\left(\frac{r_2}{r_{2A}}\cos\phi\right) = \arccos\left(\frac{r_1}{r_{1A}}\cos\phi\right) \qquad (4.19)$$

Equations (4.18) and (4.19) are the effect of the change of contact radius of a pitch-rolling-gear on gear meshing and are used in Section 5.1 to solve the kinematics of an example flex-gear device.

Gear meshing enforces pure rolling at the working pitch point P. This results in sliding at the contact point A between the rolling contact surfaces. This sliding is defined by the relative linear velocity of the rolling contact surfaces at point A. This relative velocity, referred to as *sliding velocity*, is given by

$$\Delta\overline{V}_A = \overline{V}_{A1} - \overline{V}_{A2} = \overline{\omega}_1 \times \overline{R}_1 - \overline{\omega}_2 \times \overline{R}_2 \qquad (4.20)$$

where $\overline{V}_{A1}$ and $\overline{V}_{A2}$ are, respectively, the velocity vectors of point A on gears *1* and *2*. The angular velocity vectors $\overline{\omega}_1$ and $\overline{\omega}_2$ and the contact radius vectors $\overline{R}_1$ and $\overline{R}_2$ are defined in Figure 4.10. A clockwise positive sign convention is adopted for angular velocity. Applying the right hand rule to the cross products in Equation (4.20), the linear velocities $\overline{V}_{A1}$ and $\overline{V}_{A2}$ are positive rightward, as shown in Figure 4.10. Sliding at the contact point A is the result of the mismatch of contact pitches of mating pitch-rolling-gears. The mechanical power loss from the sliding between rolling contact surfaces is discussed in Chapter 5.

In summary, the contact radius of a pitch-rolling-gear can be resized by either changing the number of teeth or allowing the contact pitch to vary. Changing the number of teeth maintains pure rolling between the rolling contact surfaces, while allowing the variance of contact pitch produces sliding. Both of these options will be considered in the application of pitch-rolling-gears to flex-gear devices in the following subsection.

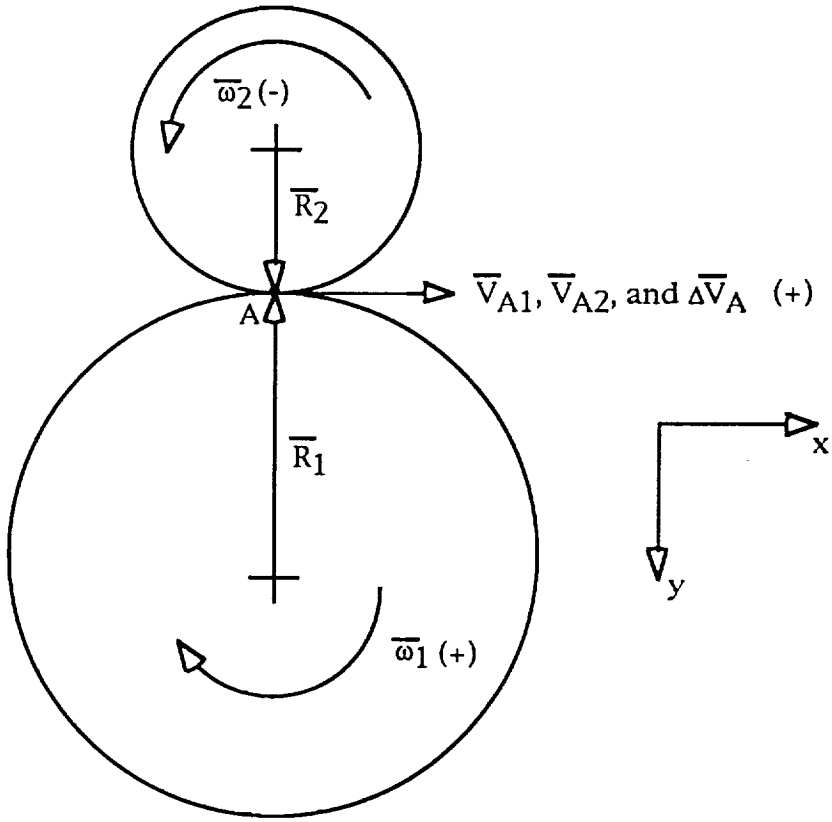

Figure 4.10: Kinematic Sign Convention

4.2.3 Flex-gear Devices

Consider applying pitch-rolling-gears to the planetary flex-gear device shown in Figure 3.2. The annulus dimension D is given by

$$D = R_3 - R_1 \tag{4.21}$$

The planet deflection δ and contact radius R_2 (previously denoted by R) were determined by the optimization in Chapter 3. These parameters require that the annulus dimension be

$$D = 2R_2 - \delta \tag{4.22}$$

First, consider an *uncompressed flex-gear device*, whose planets fit perfectly in the annulus of the sun and ring gears. Then, the planet deflection δ equals zero, and by Equation (4.22), the planet diameter $2R_2$ equals the annulus dimension D. If the contact circles coincide with the pitch circles, the pitch radii r_i equal the contact radii R_i, and

$$p = p_c = \frac{2\pi R_1}{N_1} = \frac{2\pi R_2}{N_2} = \frac{2\pi R_3}{N_3} \tag{4.23}$$

where subscripts *1*, *2*, and *3* indicate parameters of the sun, planet, and outer ring gear, respectively.

Consider an uncompressed flex-gear device with the same parameters as the example device (except $\delta = 0$). A gear pitch $p = 0.0628''$ is recommended in Section 4.1, and the planet contact

radius $R_2=0.70"$ is recommended in Chapter 3. The outer ring radius R_3 is given as approximately 3 inches in Section 1.3. Using these values in Equations (4.23), the radii R_1 and R_3 and the number of teeth N_1 and N_3 are solved, while constraining N_1 and N_3 to integer values and R_3 close to 3 inches. The result is: R_1=1.6", R_2=0.70", R_3=3.0", N_1=160, N_2=70, and N_3=300.

Now, consider compressing the planet gear by an amount δ, as recommended in Chapter 3. This planet deflection can be produced by slightly changing the contact radii R_i of the uncompressed flex-gear device. The contact radii of the planet or sun gears can be increased, or that of the outer ring gear can be decreased. As explained in Subsection 4.2.2, the contact radius of a pitch-rolling-gear can be changed, either by changing the number of teeth or by allowing the contact pitch to vary.

Ideally, the contact pitches of the sun, planet, and outer ring gears are the same for any desired planet deflection, so that zero sliding occurs between the rolling contact surfaces. However, by Equations (4.21) through (4.23), it is impossible to maintain the same contact pitches and the desired deflection δ without changing the number of teeth. So to attain the same contact pitches for the gears of a compressed planet device, consider changing the number of teeth on the gears of an uncompressed flex-gear device.

Changing the number of teeth of a pitch-rolling-gear while maintaining a constant contact pitch, changes the contact radius incrementally, as mentioned in Subsection 4.2.2. Therefore, it is

unlikely that the number of teeth N_1, N_2, and N_3 can be found to exactly yield the desired planet deflection δ. Instead, possible planet deflections are sought by changing the number of teeth, N_1, N_2, and N_3. Combining Equations (4.21) and (4.22), the planet deflection is given by

$$\delta = 2R_2 - D = 2R_2 - (R_3 - R_1) \qquad (4.24)$$

Hence, the smallest possible deflection δ occurs for the smallest change in the sun or ring radii or planet diameter. By Equation (4.23), the contact radius of any gear changes by the same increment for the same change in the number of teeth. By adding a tooth while maintaining a constant contact pitch, the contact radius of any gear with a pitch of $p=0.0628$ inches, increases by 0.010 inches. The change in radius of the planet has twice the effect on the deflection δ, according to Equation (4.24). Therefore, the smallest planet deflection is realized by adding a tooth to the sun gear or removing one from the outer ring gear. The resulting planet deflection δ of the example device equals 0.010 inches, by Equation (4.24).

The resulting flex-gear device is free from sliding between the rolling contact surfaces, since the contact pitches of the gears match. However, the planet deflection of 0.010 inches is greater than the 0.004 inches suggested in Chapter 3, for the example device. The corresponding compressive force W, by Equation (3.5), is 7.25 pounds-force, which is 4.25 pounds-force higher

than suggested in Chapter 3. Since this compressive force is excessively high for the example device, at least two options remain. One is to lower the gear pitch given in Section 4.1. This decreases the effect of changing the number of teeth on the planet deflection δ. The cost of lowering the gear pitch is lowering the duration of contact λ, as seen from Equation (4.3).

The second option is to design a device that accepts a small amount of sliding between its rolling contact surfaces. A small amount of sliding between rolling contact surfaces may cause only a negligible amount of wear and debris. However, sliding causes frictional forces that contribute to mechanical power loss in the device.

Both options are specified in Table 4.2, with the uncompressed device. With the recommended deflection and compressive force, the device in the second column accepts some sliding between its rolling contact surfaces, and is therefore referred to as a *sliding device*. Accepting a higher deflection and compressive force, the example in the third column produces pure rolling on its rolling contact surfaces, and is therefore referred to as a *rolling device*. The planet deflection of both devices is produced by oversizing the contact radius of the sun gear of the uncompressed device. The sliding device oversizes the sun gear contact radius of the uncompressed device, while maintaining the same number of teeth, allowing the contact pitch of the sun gear to change. The rolling device

pressure angle		ϕ	20°	
tooth height		a	0.025"	
tooth thickness		t	0.023"	
gear pitch		p	0.0628"	
		Uncompressed device	Sliding device	Rolling device
Sun gear:				
number of teeth	N_1	160	160	161
gear pitch radius	r_1	1.600"	1.600"	1.610"
contact radius	R_1	1.600"	1.604"	1.610"
contact pitch	p_{c1}	0.0628"	0.0630"	0.0628"
Planet gear:				
number of teeth	N_1	70	70	70
gear pitch radius	r_2	0.700"	0.700"	0.700"
contact radius	R_2	0.700"	0.700"	0.700"
contact pitch	p_{c2}	0.0628"	0.0628"	0.0628"
Outer ring gear:				
number of teeth	N_1	300	300	300
gear pitch radius	r_3	3.000"	3.000"	3.000"
contact radius	R_3	3.000"	3.000"	3.000"
contact pitch	p_{c3}	0.0628"	0.0628"	0.0628"
		———	———	———
planet deflection	δ	0	0.004"	0.010"
compressive force	W	0	3 lbf	7.3 lbf

Table 4.2: Specifications of Example Flex-gear Devices

oversizes the sun gear contact radius of the uncompressed device, while adding one gear tooth to maintain the same sun gear contact pitch.

For the example device designed throughout this thesis, the preferred configuration from Table 4.2 is the sliding device, since it offers the recommended compressive force of 3 pounds-force. The sliding device will be analyzed for average frictional torque and maximum gear stress in Chapter 5.

Pitch-rolling-gears, discussed in this subsection, are difficult to apply to a planetary type flex-gear device because of the constraint of Equation (4.21). A rack and pinion type device, as shown in Figure 4.11, does not pose this difficulty because Equation (4.21) does not apply. Thus, the deflection δ of the pinion does not depend on the contact pitch. While a planetary type device applies to rotary joints, a pinion type device applies to prismatic joints.

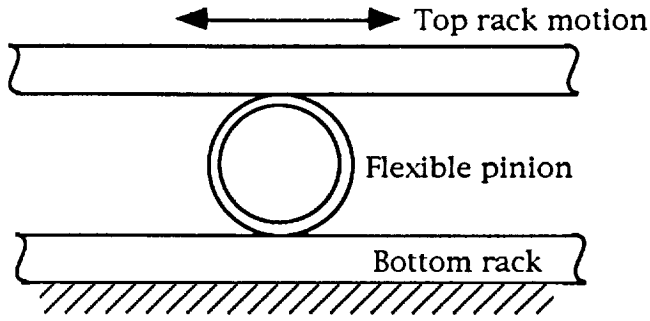

Figure 4.11: Rack and Pinion Type Flex-gear Device

CHAPTER 5

ANALYSIS OF A FLEX-GEAR DEVICE

The kinematics and kinetics of the sliding device, which is specified in Table 4.2, are presented in Sections 5.1 and 5.2. In these sections, the mechanical power loss from sliding between the rolling contact surfaces is discussed. Gear stress is discussed in Section 5.3.

5.1 Kinematics

Figure 5.1 shows a planetary flex-gear device. The *fictitious arm*, denoted by the letter a, will be used to find the angular velocities of the device. The contact point between the planet and outer ring gears is denoted by the letter B to distinguish it from the contact point A between the planet and sun gears. Accordingly, the parameters involved with planet and sun gear meshing are denoted by the subscript A. Similarly, all parameters involved

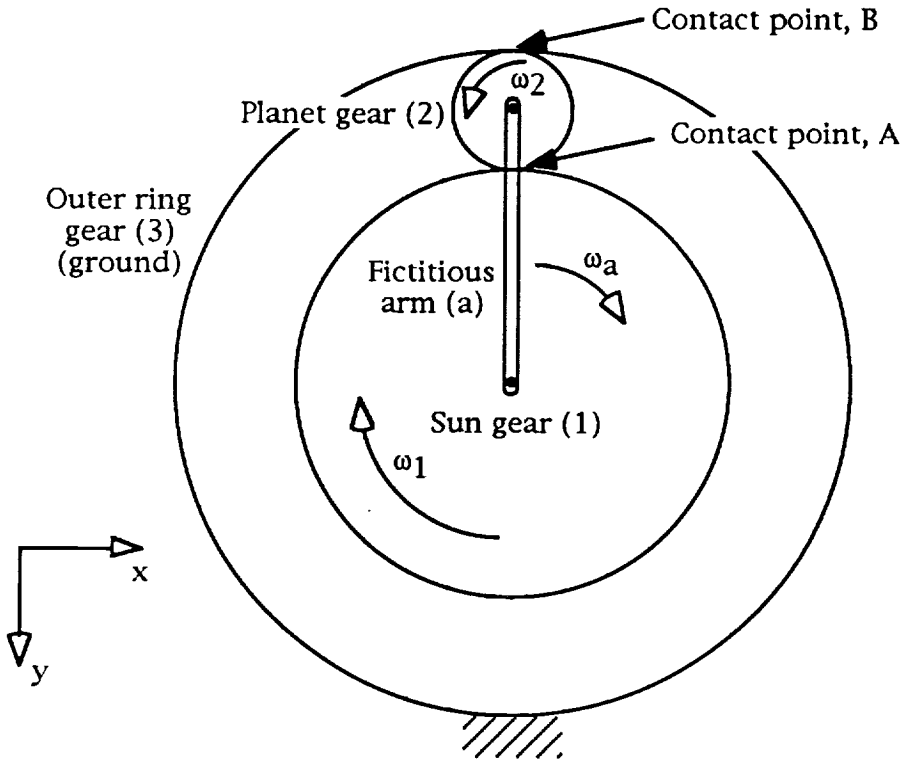

Figure 5.1: Angular Velocities of a Planetary Flex-gear Device

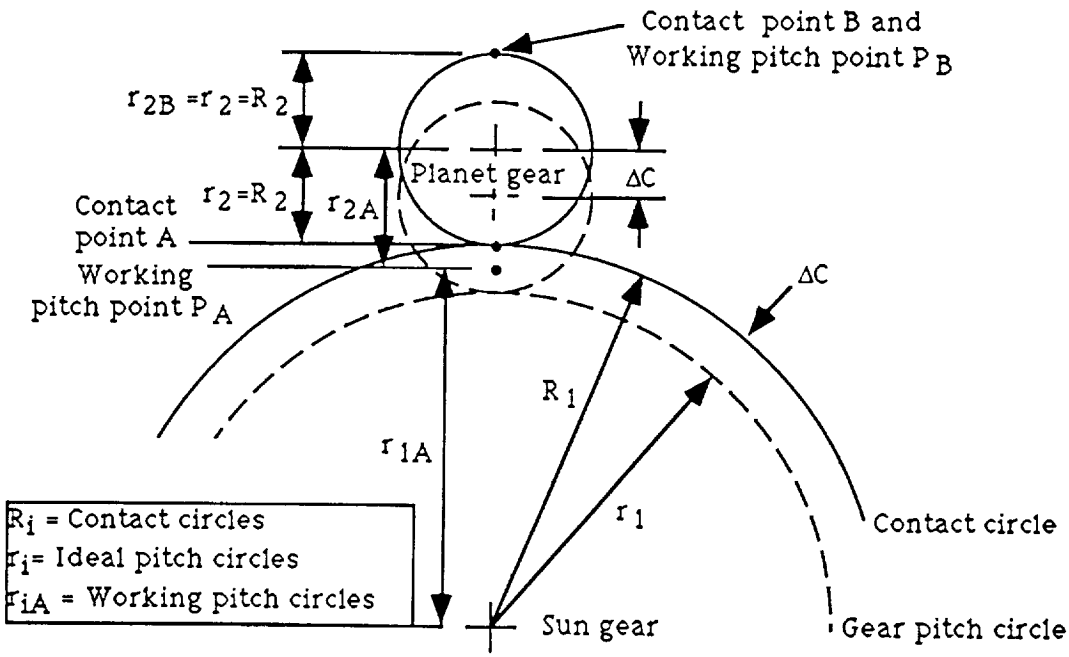

(a) Oversizing the Sun Contact Radius

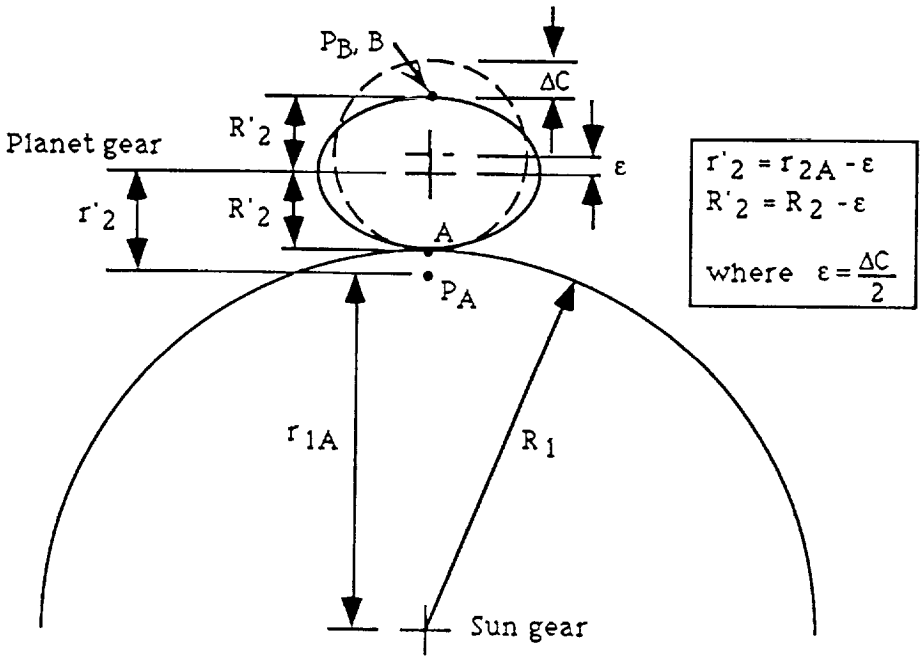

(b) Compressing the Planet

Figure 5.2: Creating the Sliding Device in Two Steps

with planet and outer ring gear meshing are denoted by the subscript B.

As stated in Chapter 4, the sliding device is the same as the uncompressed device with an oversized sun contact circle and, therefore, a compressed planet gear. Oversizing the contact circle of the sun gear and compressing the planet gear are considered in two separate steps in this section to determine the kinematics of the sliding device.

As shown in Figure 5.2a, the first step increases the contact radius of the sun gear by a distance $\Delta C = 0.004''$, from r_1 to R_1. Ignoring planet gear compression in this step, the planet is pushed up by the distance ΔC. The effect of changing the contact radius of the sun gear on sun and planet gear meshing is presented in Subsection 4.2.2. The working pitch radii, corresponding to the working pitch point P_A between the planet and sun gears, are given by Equation (4.18) as

$$r_{1A} = \frac{160}{160+70}(2.3+0.004) = 1.6028''$$

$$r_{2A} = \frac{70}{160+70}(2.3+0.004) = 0.7012''$$

And, the working pressure angle ϕ_A, corresponding to the working pitch point P_A, is given by Equation (4.19) as

$$\phi_A = \arccos\left(\frac{0.700}{0.7012}\cos(20°)\right) = 20.27°$$

The working pitch radii, corresponding to the working pitch point P_B, between the planet and outer ring gears, are the same as the gear pitch radii, since the working pitch point P_B is coincident with the contact point B:

$$r_{2B} = r_2 \tag{5.1a}$$

$$r_{3B} = r_3 \tag{5.1b}$$

Similarly, the working pressure angle ϕ_B, corresponding to the working pitch point P_B, is the same as the pressure angle $\phi = 20°$.

In the second step, shown in Figure 5.2b, the planet is compressed by the outer ring gear (not shown) at point B, by a distance ΔC. This step puts point B back to its original position, before the first step. By Subsection 4.2.1, the locations of the working pitch points P_A and P_B do not change through gear compression, relative to contact points A and B, respectively. However, the contact and working pitch radii of the planet gear are compressed. The compressed radii, denoted by primes, are less than the uncompressed radii by a distance ε. Hence, the compressed contact and working pitch circle radii of the planet, corresponding to meshing with the sun gear, are given by

$$R_2' = R_2 - \varepsilon \tag{5.1c}$$

$$r_{2A}' = r_{2A} - \varepsilon \tag{5.1d}$$

where ε is the distance that the center of the planet moves by compression. Since point B compresses the planet by ΔC, the distance ε is half of ΔC. The compressed contact and working pitch circle radii of the planet, corresponding to meshing with the outer ring gear, are given by

$$R_2' = R_2 - \varepsilon \tag{5.1e}$$

$$r_{2B}' = r_{2B} - \varepsilon = r_2 - \varepsilon \tag{5.1f}$$

The compressed working pitch radii r_{2A}' and r_{2B}' of the planet gear determine the relative angular velocities of the gears in the flex-gear device. All the kinematic parameters of the sliding device are presented in Table 5.1.

The device, shown in Figure 5.1, can be operated by rotating the sun gear (1) with respect to the outer ring gear (3) or vice versa. In a robot joint, it is assumed that the sun gear is rotating with respect to the outer ring gear. To derive the angular velocities of the device relative to the outer ring, the angular velocities relative to the fictitious arm are found. In the following, the notation $\omega_{i/j}$ denotes the angular velocity of body i with respect to body j.

By Equation (4.17), the angular velocity of the planet gear with respect to the fictitious arm is

$$\omega_{2/a} = -\frac{\omega_{1/a} r_{1A}}{r_{2A}'} \tag{5.2a}$$

Parameter	Equation used	Value
Sun gear:		
r_{1A}	4.18a	1.6028"
ϕ_A	4.19	20.27°
Planet gear:		
r_{2A}	4.18b	0.7012"
r_{2B}	5.1a	0.7000"
r'_{2A}	5.1d	0.6992"
r'_{2B}	5.1f	0.6980"
R'_2	5.1c	0.6980"
Outer ring gear:		
r_{3B}	5.1b	3.0000"
ϕ_B	4.19	20°

Table 5.1: Kinematic Parameters of the Sliding Device

In accordance with Subsection 4.2.1, the change in the angular velocity throughout the planet gear from deformation is neglected, so that the angular velocity is constant throughout the planet gear. By the definition of angular velocity, the linear velocity of the pitch point P_B between the planet and outer ring gears, with respect to the fictitious arm, is given by

$$V_{2B} = \omega_{2/a} r'_{2B} = -\frac{\omega_{1/a} r_{1A}}{r'_{2A}} r'_{2B} \tag{5.2b}$$

Since the linear velocity of P_B is the same on both the planet and outer ring gears, the angular velocity of the outer ring gear, with respect to the fictitious arm, is

$$\omega_{3/a} = \frac{V_{2B}}{r_3} = -\frac{\omega_{1/a} r_{1A} r'_{2B}}{r'_{2A} r_3} \tag{5.2c}$$

Subtracting $\omega_{3/a}$ from $\omega_{1/a}$ and $\omega_{2/a}$, the angular velocities of the sun and planet gears with respect to the ring are obtained:

$$\omega_{1/3} = \omega_{1/a} - \omega_{3/a} = -\omega_{1/a}\left(1 + \frac{r_{1A} r'_{2B}}{r'_{2A} r_3}\right) \tag{5.2d}$$

$$\begin{aligned} \omega_{2/3} = \omega_{2/a} - \omega_{3/a} &= \omega_{1/a}\left(-\frac{r_{1A}}{r'_{2A}} + \frac{r_{1A} r'_{2B}}{r'_{2A} r_3}\right) \\ &= \omega_{1/3}\left(\frac{-\frac{r_{1A}}{r'_{2A}} + \frac{r_{1A} r'_{2B}}{r'_{2A} r_3}}{1 + \frac{r_{1A} r'_{2B}}{r'_{2A} r_3}}\right) \end{aligned} \tag{5.2e}$$

The average sliding velocity between the rolling contact surfaces of the planet and outer ring gears is zero, since the contact and working pitch circles coincide with one another. The average sliding velocity between the rolling contact surfaces of the planet and sun gears, given by Equation (4.20), is

$$\begin{aligned}\Delta V_A &= \overline{\omega}_{1/a} \times \overline{R}_1 - \overline{\omega}_{2/a} \times \overline{R}_2' \\ &= \frac{\omega_{1/3} R_1}{\left(1 + \frac{r_{1A} r_{2B}'}{r_{2A}' r_3}\right)} - \frac{\omega_{1/3} r_{1A} R_2'}{\left(1 + \frac{r_{1A} r_{2B}'}{r_{2A}' r_3}\right) r_{2A}'} \\ &= \frac{\omega_{1/3}}{\left(1 + \frac{r_{1A} r_{2B}'}{r_{2A}' r_3}\right)} \left(R_1 - \frac{r_{1A} R_2'}{r_{2A}'}\right)\end{aligned} \qquad (5.3)$$

Sliding between the rolling contact surfaces at the contact point A produces a frictional force that resists the motion of the device. *Frictional torque* is defined as the torque that the frictional force exerts on the sun gear. Frictional torque is calculated at the sun gear because the sun gear is the perceived input of the device. By energy equivalence, the mechanical power loss from sliding between the rolling contact surfaces is given by

$$\textit{mechanical power loss} = T \cdot \omega_{1/3} = f_A \Delta V_A \qquad (5.4a)$$

where T is the frictional torque at the sun gear, and f_A is the sliding friction force between the sun and planet gears at the contact point A. The frictional torque is solved from Equation

(5.4a) and denoted by T_{nrg}, to indicate that it has been calculated by energy equivalence:

$$T_{nrg} = f_A \frac{\Delta V_A}{\omega_{1/3}} \qquad (5.4b)$$

The friction force f_A is solved in the following subsection.

5.2 Kinetics

To investigate the kinetics of the sliding flex-gear device, the free body diagrams of the sun and planet gears are constructed in Figure 5.3. All the dimensions, therein, are taken from Figure 5.2b. Inertial terms are neglected.

The sliding friction force f_A, at the contact point A, develops from sliding between the rolling contact surfaces. Substituting the values of Table 5.1 into Equation (5.3), yields

$$\Delta V_A = \omega_{1/3}\left[\frac{1.6040 - \dfrac{0.6980 \cdot 1.6028}{0.6992}}{1 + \dfrac{0.6980 \cdot 1.6028}{0.6992 \cdot 3.0000}}\right] = 0.00257\,\omega_{1/3}$$

Unsurprisingly, the magnitude and direction of the sliding velocity ΔV_A is directly dependent on the magnitude and direction of the angular velocity of the sun gear, $\omega_{1/3}$.

In accordance with the sign convention defined in Figure 4.10, a positive (clockwise) sun gear rotation is adopted in Figure 5.3. This results in a positive (rightward) sliding velocity ΔV_A at

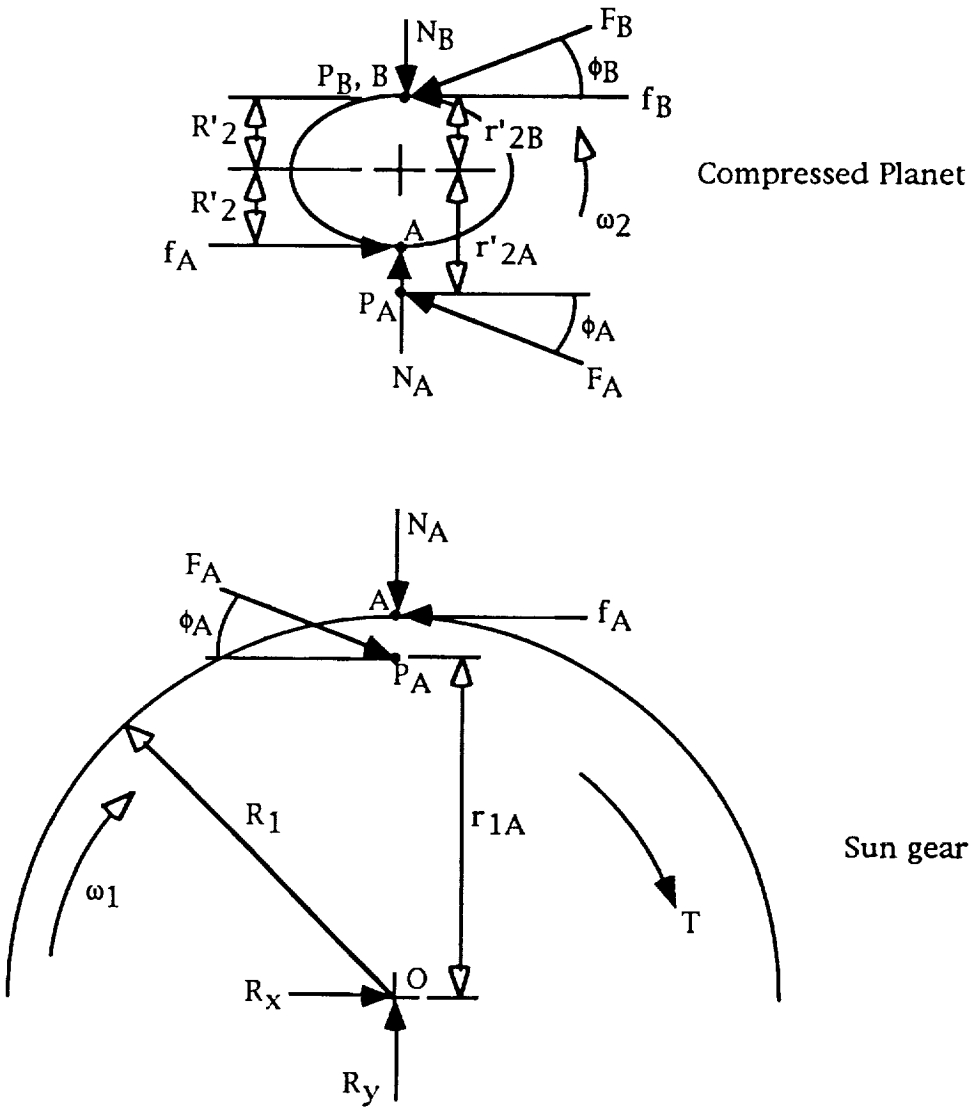

Figure 5.3: Free Body Diagram of Sliding Device

the contact point A, producing an opposite (leftward) frictional force f_A on the sun. An equal and opposite force occurs on the planet gear at the same point, A. Summing the moments on the planet gear about B indicates the direction of the gear force F_A. This gear force acts at the working pressure angle ϕ_A, given in Table 5.1. The frictional force f_A and gear force F_A apply a torque to the planet gear that can only be balanced by the frictional and gear forces at point B.

Summing the moments on the planet gear about point A indicates the directions of the frictional and gear forces through point B, as shown in Figure 5.3. Both the gear force F_B and the frictional force f_B can act simultaneously. However, the gear force F_B acts only when the gearing surfaces between the planet and outer ring gears are in contact. Assuming some mechanical backlash between the gearing surfaces of the device, the gearing surfaces between the planet and outer ring gears do not touch, since pure rolling occurs at point B. For this reason, only the static frictional force f_B acts at point B. If the maximum frictional force determined by the coefficient of friction is, however, not enough to keep the planet in equilibrium, the gear force F_B will also act.

As shown in Figure 5.3, the normal forces N_A and N_B must be compressive due to the nature of surface contact. Finally, the reaction forces R_x and R_y constrain the center of the sun gear, and the input torque T assumes a positive or clockwise direction.

Physically, because the contact circle of the sun gear is greater than its working pitch circle, torque is transmitted from the sun to the planet via friction at the contact point A. To prevent the planet from running out of position, the mating gear teeth produce a force opposite to the frictional force at P_A, as shown in Figure 5.3. The mechanics of this device are remarkably different from that of a standard gear device.

The equilibrium solution of a compressed planet device is approximate, because the change of the angle and location of the gear forces through planet compression are not accounted for, as justified in Subsection 4.2.1. Ignoring the gear force F_B, there are 8 unknowns T, R_x, R_y, F_A, N_A, N_B, f_A, and f_B in Figure 5.3. To solve for these unknowns, two equations, in addition to the 3 equations of equilibrium (in the plane of the device) for each gear, must be used. The first equation is supplied by the dry friction model:

$$f_A = \mu N_A \tag{5.5}$$

where μ is the coefficient of friction. For the example device, $\mu = 0.5$ is conservatively assumed for non-lubricated operation. The second equation, coming from the compliance of the planet gear, is Equation (3.5). In that equation, the compressive force W represents the sum of the vertical components of the forces between mating gears, i.e.,

$$W = N_A + F_A \sin\phi_A \tag{5.6}$$

With Equations (5.5) and (5.6), the 8 unknowns can be solved in terms of the known compressive force W. The torque solved by equilibrium is denoted by T_{eql} and compared to the torque solved by energy equivalence T_{nrg}, from the previous subsection. Summing the moments of the planet about B, yields

$$2f_A R_2' = F_A(R_2' + r_{2A}')\cos\phi_A \qquad (5.7)$$

Summing the moments of the sun about O, yields

$$T_{eql} = f_A R_1 - F_A r_{1A}\cos\phi_A \qquad (5.8)$$

Combining equations (5.5) through (5.8), yields

$$F_A = \frac{2\mu W R_2'}{2\mu\, R_2'\sin\phi_A + (R_2' + r_{2A}')\cos\phi_A} \qquad (5.9a)$$

$$N_A = W - F_A\sin\phi_A \qquad (5.9b)$$

$$f_A = \mu(W - F_A\sin\phi_A) \qquad (5.9c)$$

and,

$$T_{eql} = \mu(W - F_A\sin\phi_A)(r_1 + \Delta C) - F_A r_{1A}\cos\phi_A \qquad (5.9d)$$

Substituting the frictional force f_A from Equation (5.9c) into Equation (5.4b), the frictional torque by energy equivalence T_{nrg} is solved. T_{nrg} is equivalent to T_{eql}, which is given by Equation (5.9d). For the kinematic values given in Table 5.2, the frictional torque T is

$$T = T_{nrg} = T_{eql} = 0.0033 \text{ in} \cdot \text{lbf} \tag{5.10}$$

Summing the forces on the planet in the horizontal direction, yields

$$f_B = f_A - F_A \cos\phi_A \tag{5.11}$$

Summing the forces on the planet in the vertical direction, yields

$$N_B = W \tag{5.12}$$

The summation of forces on the sun gear yields the reaction forces R_x and R_y, whose solutions are not presented in this thesis.

Values of the equilibrium solution of the sliding flex-gear device are listed in Table 5.2. Notice that the normal force N_A, at the rolling contact between the planet and the sun gear, is considerably less than the compressive force W. This somewhat lessens the contact area of the model in Chapter 3. The frictional force f_B is extremely small, because it acts only to balance the

Force	Equation	Value
W	given	3.0000 lbf
F_A	5.9a	1.3488 lbf
N_A	5.9b	2.5327 lbf
f_A	5.9c	1.2663 lbf
T	5.10	0.0033 in-lbf
f_B	5.11	0.0011 lbf
N_B	5.12	3.0000 lbf

Table 5.2: Equilibrium Solution of the Sliding Device

small moment from gear meshing at point A, which is relatively far away.

Additional mechanical power is lost from sliding between the involute gearing surfaces. Sliding between the gearing surfaces of pitch-rolling-gears is similar to that of standard gears. By energy equivalence,

$$mechanical\ power\ loss = T_G\,\omega_{1/3} = (f_t V_r)_A + (f_t V_r)_B \qquad (5.13)$$

where T_G is the frictional torque contributed from sliding between the gearing surfaces, V_r is the relative velocity of mating gearing surfaces at their instantaneous points of contact, and f_t is the corresponding frictional force between mating gear teeth. Frictional torque from gearing surface sliding is not calculated in this thesis.

5.3 Stress in the Sliding Device

A flexible planet gear is subjected to more stress than both the solid sun and outer ring gears. In addition to the local deformation from rolling surface contact that all the gears undergo, the planet is subjected to global deformation, due to compression. Furthermore, the slim addendum teeth of the addendum planet gear are subjected to more stress, from tooth loading, than the thicker dedendum teeth of the sun and outer ring gears. The local, global, and tooth stresses of the planet are investigated in this section.

The local deformation of the planet from rolling surface contact was modeled by the Hertz contact theory in Section 3.1.3. The coordinates for the contact regions of the planet with both the sun and outer ring gears are shown in Figure 5.4. By the Hertz contact theory, which neglects friction, the stress of a contact region is highest along the z-axis, where the normal stresses are given by Sidebottom and Boresi [1970] as

$$\sigma_x = -\frac{b\left[\sqrt{1+\left(\frac{z}{b}\right)^2}-\frac{z}{b}\right]^2}{\Delta\sqrt{1+\left(\frac{z}{b}\right)^2}} \qquad (5.14a)$$

$$\sigma_y = -\frac{2b\nu_2}{\Delta}\left[\sqrt{1+\left(\frac{z}{b}\right)^2}-\frac{z}{b}\right] \qquad (5.14b)$$

$$\sigma_z = -\frac{b}{\Delta\sqrt{1+\left(\frac{z}{b}\right)^2}} \qquad (5.14c)$$

where ν_2 is Poisson's ratio of the planet gear material. For the rolling surface contact between the planet and the sun gear,

$$b = \sqrt{\frac{2N_A\Delta}{\pi d}} \qquad (5.15a)$$

$$\Delta = \frac{\left(\frac{1-\nu_1^2}{E_1}+\frac{1-\nu_2^2}{E_2}\right)}{\frac{1}{2r_1}+\frac{1}{2\rho}} \qquad (5.15b)$$

For the rolling surface contact between the planet and the outer ring gear,

$$b = \sqrt{\frac{2N_B \Delta}{\pi d}} \tag{5.16a}$$

$$\Delta = \frac{\left(\frac{1-\nu_2^2}{E_2} + \frac{1-\nu_3^2}{E_3}\right)}{\frac{1}{2\rho} + \frac{1}{2r_3}} \tag{5.16b}$$

The highest state of normal stress, for any contact region, occurs at the contact point *(z=0)*. For the example sliding device, the highest stress state occurs between the planet and the outer ring gears. This stress state has a maximum normal stress of 17,000 psi and an octahedral stress of 15,000 psi.

As mentioned in Section 3.1, the Hertz contact theory was derived for two solid semi-infinite bodies in contact. Hence, any additional stress, from the global deformation of the planet, must be accounted for separately.

Global deformation of the planet is modeled in Section 3.1.2 by a thin ring compressed by two diametrically opposing point loads. Young [1989] presents the resulting bending moment, hoop load, and shear force, defined in Figure 5.5. The internal bending moment is given by

$$M = WR\left[\frac{1}{\pi}\left(1-\frac{c^2}{12R^2}\right) - \frac{\sin x}{2}\right] \qquad (5.17a)$$

The hoop or normal load is given by

$$H = -\frac{W}{2}\sin x \qquad (5.17b)$$

Finally, the shear force is given by

$$V = -\frac{W}{2}\cos x \qquad (5.17c)$$

Since the radius R of the planet gear is much greater than the thickness c, the stress in the planet can be determined from the bending, hoop, and shear loads, by beam theory. The bending stress is given by

$$\sigma_b = \frac{M\,y}{I} \qquad (5.18)$$

where I is the area moment of inertia, given in Section 3.1.2 as $I = d\,c^3/12$. The hoop stress is

$$\sigma_h = \frac{H}{A} \qquad (5.19)$$

where A is the cross sectional area $A = d\,c$. The total x-normal stress is the sum of the bending and hoop stresses:

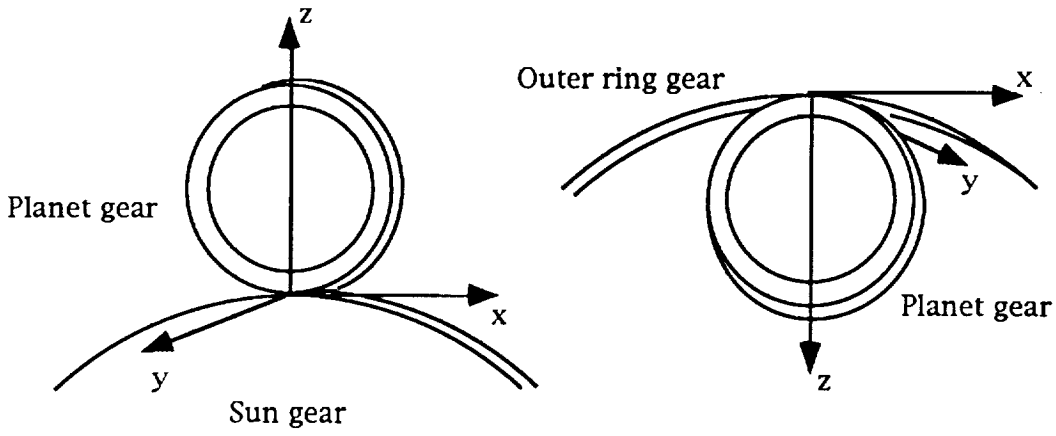

(a) Contact between Sun and Planet Gears

(b) Contact between Outer Ring and Planet Gears

Figure 5.4: Coordinates Local to Contact

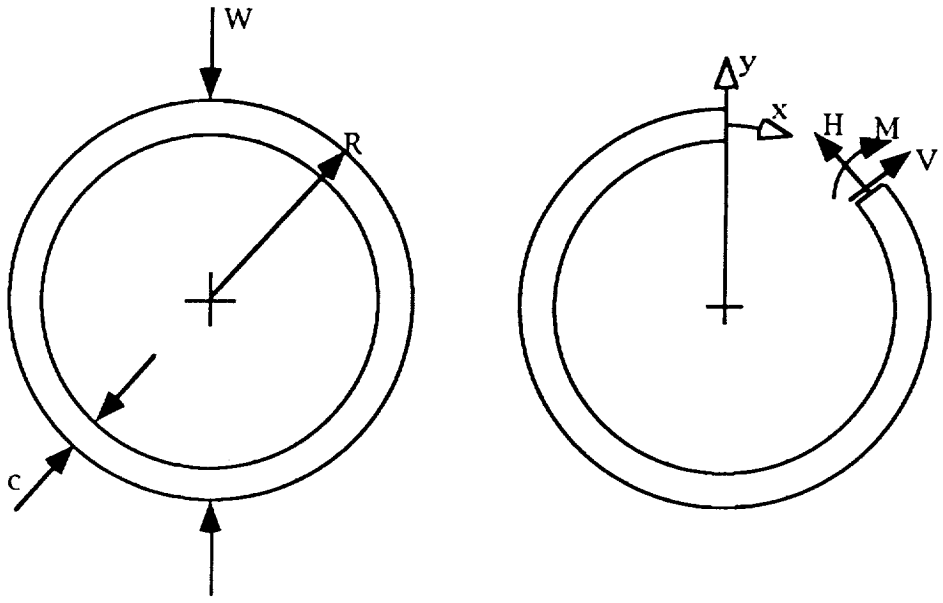

Figure 5.5: Definition of Bending, Hoop, and Shear

$$\sigma_x = \sigma_b + \sigma_h \tag{5.20}$$

For the example sliding device, the maximum x-normal stress occurs at $x=\pm\pi/2$ and is equal to 12,000 psi.

In accordance with Young [1989], the radial or y-normal stress for the example flex-gear device can be ignored. The shear stress τ of the planet gear is approximated by the parabolic distribution of a straight beam, whose maximum shear stress occurs at the center of the beam, and is given by

$$\tau_{max} = \frac{3}{2}\frac{V}{A} \tag{5.21}$$

For the example sliding device, the maximum shear stress occurs at $x=0,\ \pi$ and is equal to 150 psi.

Finally, tooth stress is investigated. A loaded tooth of the planet gear is shown in Figure 5.6. Friction, arising from the gear force F, is neglected in the calculation of gear tooth stress. The angle, at which the gear force F acts with respect to the tooth, is the pressure angle ϕ_a at the top of the tooth, and is given by [Kimbrell, 1991] as

$$\phi_a = \arccos\left(\frac{R}{R_a}\cos\phi\right) \tag{5.22}$$

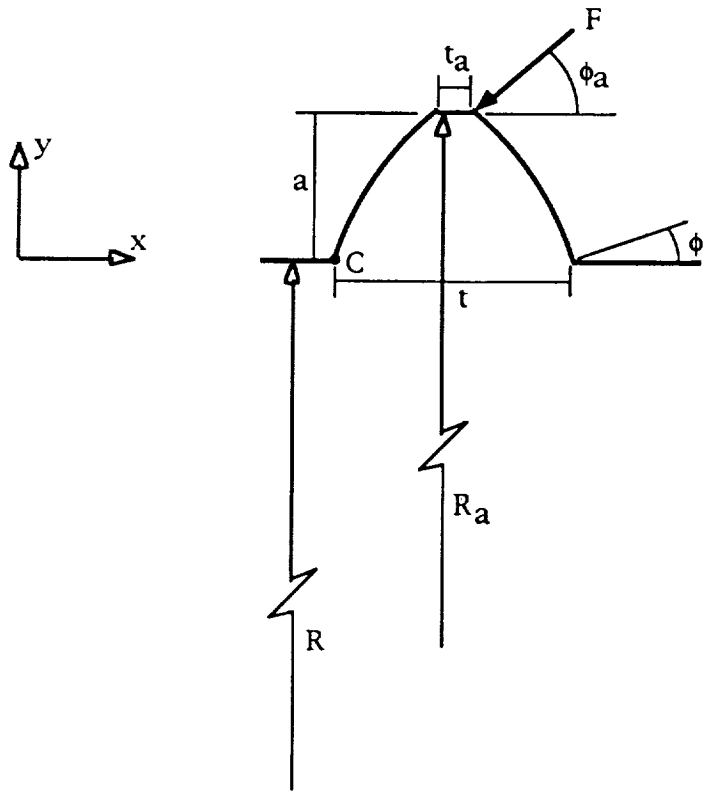

Figure 5.6: Planet Tooth Loading

This pressure angle should not be confused with the working pressure angle ϕ_A used in the study of gear meshing. For the example device, the pressure angle ϕ_t at the top of the tooth is 24.9°.

Rather than finding the entire stress field, critical stresses, at specific points, are checked. Stress at point C, as shown in Figure 5.6 arises from tooth bending, compression, and shear. The compressive stress at point C is

$$\sigma_c = \frac{F \sin \phi_t}{t\, d} \tag{5.23a}$$

where d is the depth of the tooth into the page (the axial thickness of the gear). Approximating the tooth as a beam, the bending stress at point C is

$$\sigma_b = \frac{M\, t/2}{I} \tag{5.23b}$$

where the moment of inertia $I = d\, t^3/12$, and the bending moment $M = a\, F \cos \phi_t$. Finally, the shear stress at point C is given by

$$\tau = \frac{F \cos \phi_t}{t\, d} \tag{5.23c}$$

In the sliding device, the higher gear force occurs between the sun and planet gears. For this gear force, F_A, the stress state at point C has an octahedral stress of only 10,000 psi.

The shear stress at the top of the addendum tooth is

$$\tau_a = \frac{F\cos\phi_a}{t_a\, d} \qquad (5.24)$$

For the gear force F_A, given in Table 5.2, and an addendum tooth thickness of $t_a = 0.003"$, from Chapter 4, the shear stress $\tau_a = 2500 psi$.

In summary, the stresses of the sliding device are low. The stress due to rolling surface contact is highest, but still well within the range of strengths offered by beryllium-copper alloys.

CHAPTER 6

CONCLUDING REMARKS

In conclusion, flex-gears offer a strong alternative of transferring electricity across continuously rotating joints. The flex-gear devices that are developed in this thesis are expected to transfer more electricity than roll rings, while incurring less wear than brushes. Flex-gears may serve as a standard in space applications in the near future.

6.1 Summary

In this thesis a new class of gears, called pitch-rolling-gears, is developed for use in flex-gear devices. These gears are designed to transfer electrical power, whereas standard gears are designed to transfer mechanical power. A pitch-rolling-gear uses involute gearing surfaces, similar to those of a standard gear, to maintain

its position with respect to its mating gear. Additionally, pitch-rolling-gears employ rolling contact surfaces, similar to those of roll-rings to transfer electricity. Pitch-rolling-gears, used as the flexible planet gears in a planetary gear device, maintain their position in the annulus of the sun and outer ring gears. In this way, multiple planet gears can be used to substantially increase the current carrying capability of the device.

The capability of the gearing surfaces to maintain gear position is independent of the performance of the rolling contact surfaces to conduct electricity. Consequently, the gearing and rolling contact surfaces are separately designed to maximize the current carrying capability of the device.

Current carrying capability is defined by the contact area between the rolling contact surfaces of mating pitch-rolling-gears. Two theoretical models are developed to predict this contact area as a function of planet radius. The closed-form and finite element models are in close agreement. From the closed-form model, the optimum radius of the planet gear is chosen for the example flex-gear device.

The gearing surfaces are designed to maximize the duration of contact between mating rolling contact surfaces. The duration of contact available on an addendum planet gear is found through geometry. For the planet of the example device, whose radius was determined from the maximization of current carrying capability, gear tooth size is chosen to maximize the available duration of contact. Corresponding sun and outer ring gears are

specified to produce the planet compression that is specified in Chapter 3.

To find the friction torque and gear stress of any pitch-rolling-gear device, the kinematics and kinetics of pitch-rolling-gears are analyzed in Chapter 4. The effects of changing the contact and pitch radii of a pitch-rolling-gear on gear meshing are determined. The effect of compressing a pitch-rolling-gear on gear meshing is discussed, and its effect on kinetics is neglected. The frictional torque and gear stress, for the example device specified in Chapter 4, are shown in Chapter 5 to be well within acceptable limits.

6.2 Recommendations for Future Work

Throughout the optimization of the flexible planet in the example device, three significant assumptions are made.

Foremost, the basis of the optimization of planet gear size is the approximation that Hertz contact area predicts the area through which electricity flows. The area for electrical flow may actually be less than the Hertz area, especially for extremely thin rings, whose contact pressure is thought to be less than solid cylinders in contact. The flex-gear device can be further optimized through a better understanding of electrical contact. An experimental study of the current carrying capability of thin rings is recommended.

The second assumption is the value of the minimum planet thickness required to limit planet tooth deflection. To improve

the current carrying capability of the example flex-gear device, a smaller planet thickness can be used. For this reason, the search for the dependence of tooth deflection on planet thickness is suggested.

Finally, a standard gear pressure angle of 20° is adopted in Chapter 4 for the example flex-gear device. A higher pressure angle would increase the duration of contact between the rolling contact surfaces and decrease gear forces, thereby decreasing frictional torque. The benefit of increasing the pressure angle should be weighed against the cost of using a non-standard pressure angle.

Perhaps, the most profound improvement in current carrying capability of flex-gears can be made by finding a more flexible conductive material. A flexible material (one with a low modulus of elasticity) would allow the use of smaller planet gears to conduct more electricity, as indicated by the optimization of planet size in Chapter 3.

For the kinematic and kinetic analyses of pitch-rolling-gears, the pressure line of compressed pitch-rolling-gears is approximated by the pressure line of uncompressed gears. For pitch-rolling-gear devices, especially with a larger compression than the example devices discussed in this thesis, the actual pressure line may significantly change angle and shape. The pressure line (or curve) between flexible pitch-rolling-gears can theoretically be found while considering the global deformation of the gears. Global deformation of a thin ring (or hollow gear),

subjected to a concentrated point load, is given by Timoshenko [1936].

Axial confinement of the planet gears in the annulus of the sun and outer ring gears is not considered in this work. It is assumed in Chapter 2 that the planet gears are axially confined by smooth and hard insulating material, such as glass or ceramic. Alternatively, concave and convex rolling contact surfaces can be employed for axial confinement. This axial confinement scheme is used in roll-rings [Porter, 1985].

References

- American Society for Metals, 1978, *Metals Handbook* (Ninth Edition), Vol. 2, pp. 393-402.

- Boresi, A. P., and Sidebottom, O. M., 1970, *Advanced Mechanics of Materials* (Fourth Edition), John Wiley & Sons, New York, NY, pp. 599-642.

- Boston Gear, *Boston Gear Catalog*, Engineering Information, Boston, MA, pp. 133-153.

- Cowie, A., 1961, *Kinematics and Design of Mechanisms*, International Textbook Co., Scranton, PA, pp. 197-223.

- Holm, R., 1967, *Electrical Contacts* (Fourth Edition), Springer-Verlag, New York, NY, pp. 200-259.

- Johnson, K. L., 1985, *Contact Mechanics*, Cambridge Publishing, Boston, MA, pg. 129.

- Kimbrell, J., 1991, *Kinematics Analysis and Synthesis*, McGraw-Hill, New York, NY, pp. 258-259.

- Nakada, T., and Utagawa, M., 1956, "The Dynamic Loads on Gear Caused by the Varying Elasticity of the Mating Teeth," *Proceedings of the 6th Japan National Congress for Applied Mechanics*, Tokyo, Japan, pp. 493-497.

- Porter, R., 1985, "A Rotating Transfer Device," *19th Aerospace Mechanisms Symposium*, New York, NY, pp. 277-291.

- Shigley, J. E., and Mischke, C. R., 1989, *Mechanical Engineering Design* (Fifth Edition), McGraw-Hill, New York, NY, pp. 527-544.

- Sperry Corporation, April 1981, *Roll Rings*, Sperry Corporation publication no. 41-1720-00-05.

- Still, 1916, *Principles of Electrical Design: DC and AC Generators*, McGraw-Hill, New York, NY, pp. 178-181.

- Stolarski, T. A., 1990, Tribology in Machine Design, Industrial Press, Inc., New York, NY, pg. 69.

- Timoshenko, S., 1936, Theory of Elastic Stability, McGraw-Hill, New York, NY, pp. 204-207.

- Young, W. C., 1989, *Roark's Formulas for Stress & Strain* (Sixth Edition), McGraw-Hill, New York, NY, pp. 233-263.

Bibliography

- Beyer, W. H., *CRC Standard Mathematical Tables* (25th Edition), CRC Press, Boca Raton, FL.

- Timoshenko, S., and Goodier, J., 1970, *Theory of Elasticity* (third Edition), McGraw-Hill, New York, NY.

- Wolfram, S., 1991, *Mathematica, A System for Doings Mathematics by Computer* (Second Edition), Addison-Wesley, New York, NY.